Article:
Liang, KL, Roels, J, Lavaert, M et al. (19 more authors) (2023) Intrathymic dendritic cell-biased precursors promote human T cell lineage specification through IRF8-driven transmembrane TNF. Nature Immunology, 24. pp. 474-486. ISSN 1529-2908

https://doi.org/10.1038/s41590-022-01417-6

Intrathymic dendritic cell precursors promote human T-lineage specification via IRF8-driven transmembrane TNF

Kai Ling Liang[1,2], Juliette Roels[1,11,14], Marieke Lavaert[1,12,14], Tom Putteman[1], Lena Boehme[1], Laurentijn Tilleman[3], Imke Velghe[1], Valentina Pegoretti[4], Inge Van de Walle[1,13], Stephanie Sontag[5,6], Jolien Vandewalle[7,8], Bart Vandekerckhove[1,2], Georges Leclercq[1,2], Pieter Van Vlierberghe[2,9], Claude Libert[7,8], Filip Van Nieuwerburgh[2,3], Roman Fischer[4], Roland E Kontermann[4], Klaus Pfizenmaier[4], Gina Doody[10], Martin Zenke[5,6], Tom Taghon[1,2]

[1]Department of Diagnostic Sciences, Ghent University, Ghent, Belgium.

[2]Cancer Research Institute Ghent, Ghent, Belgium.

[3]Laboratory of Pharmaceutical Biotechnology, Ghent University, Ghent, Belgium.

[4]Institute of Cell Biology and Immunology, University of Stuttgart, Stuttgart, Germany.

[5]Institute for Biomedical Engineering, Department of Cell Biology, RWTH Aachen University Medical School, Aachen, Germany.

[6]Helmholtz-Institute for Biomedical Engineering, RWTH Aachen University, Aachen, Germany.

[7]VIB Center for Inflammation Research (IRC), Technologiepark, Ghent, Belgium.

[8]Department of Biomedical Molecular Biology, Ghent University, Ghent, Belgium.

[9]Department of Biomolecular Medicine, Ghent University, Ghent, Belgium.

[10]Leeds Institute of Medical Research, University of Leeds, Leeds, UK.

[11]Present address: Genentech Inc., South San Francisco, CA, USA.

[12]Present address: Laboratory of Genome Integrity, Center for Cancer Research, National Cancer Institute, National Institutes of Health, Bethesda, MD, USA.

[13]Present address: argenx BVBA, Zwijnaarde, Belgium.

[14]These authors contributed equally: Juliette Roels, Marieke Lavaert.

Corresponding author:

Tom Taghon

Department of Diagnostic Sciences

Ghent University

C. Heymanslaan 10

MRB2, Entrance 38

9000 Ghent, Belgium

+32 (0) 9 332 01 33

tom.taghon@ugent.be

ABSTRACT

The cross talk between thymocytes and thymic stromal cells is fundamental for T cell development. In humans, intrathymic development of dendritic cells is evident but its physiological significance is unknown. Here, we show that IRF8-dependent dendritic cell precursors express transmembrane TNF to promote differentiation of thymus seeding hematopoietic progenitors into T-lineage specified precursors through activation of TNFR2 instead of TNFR1. Furthermore, we demonstrate that *in vitro* recapitulation of TNFR2 signaling by providing low density of transmembrane TNF or a TNFR2 agonist enhances the generation of human T cell precursors. Hitherto, dendritic cells have only been described to mediate thymocyte selection and maturation. Our study establishes a physiological role for the intrathymic development of dendritic cells as a hematopoietic stromal support for the early stages of human T cell development and provide a proof-of-concept to selectively target TNFR2 to enhance the *in vitro* generation of T cell precursors for clinical application.

KEYWORDS

human thymus, dendritic cell precursors, T cell precursors, IRF8, Notch signalling, transmembrane TNF, TNFR2, hematopoietic stem and progenitor cells, in vitro T cell development, interferon signalling

INTRODUCTION

T cell development takes place in the thymus which is constantly seeded by hematopoietic progenitor cells that originate from the bone marrow. These thymus seeding progenitors (TSPs) undergo stepwise differentiation and eventual selection in order to generate a diverse T cell repertoire that responds to foreign antigens but is self-tolerant. During this multi-step developmental process, cells migrate throughout the thymus where they receive the appropriate site- and stage-specific signals through cellular contact with stromal cells in distinct thymic microenvironments. Stromal cells of non-hematopoietic origin comprise mostly thymic epithelial cells (TECs) that constitute the thymic architecture. In contrast to TECs that regulate T cell development throughout the early and late stages, stromal cells of hematopoietic origin have only been described to mediate the selection of developing T cells during final maturation. In human, these include thymus-residing dendritic cells (DCs) and B cells (Martin-Gayo et al., 2010; Nunez et al., 2016; Park et al., 2020; Watanabe et al., 2005). Intriguingly, recent studies provide compelling evidence of human in situ intrathymic development of dendritic but not B cells (Lavaert et al., 2020; Le et al., 2020; Martin-Gayo et al., 2017). The physiological relevance of this disparity is unclear given their common role in the establishment of T cell tolerance.

During early T cell development, TECs provide critical Notch ligands that allow TSPs to undergo T-lineage specification to become early T cell precursors (ETPs) (Hozumi et al., 2008; Koch et al., 2008), and also produce vital cytokines such as interleukin-7 (IL-7) to support the survival and proliferation of these immature thymocytes (Han and Zuniga-Pflucker, 2021). Recapitulation of these signals has allowed us to model and study T cell development *in vitro* (Jaleco et al., 2001; Schmitt and Zuniga-Pflucker, 2002; Seet et al., 2017). However, a role for hematopoietic stromal cells in these early T developmental stages has not yet been illustrated. Also supplementation of the soluble form of tumour necrosis factor (sTNF) to existing *in vitro*

culture systems has been reported to temporarily and dose-dependently enhance the generation of human T cell precursors from hematopoietic stem and progenitor cells (HSPCs) (Dos Santos Schiavinato et al., 2016; Edgar et al., 2022; Moirangthem et al., 2021; Smits et al., 2007; Weekx et al., 2000). Physiologically, TNF is synthesized by cells as a membrane-bound precursor (transmembrane TNF, tmTNF) that can be cleaved to yield sTNF (Black et al., 1997; Kriegler et al., 1988). The production of TNF is weakly correlated with its gene expression due to post-transcriptional and translational regulation (Azzawi and Hasleton, 1999). Although both tmTNF and sTNF are biologically active, the former is predominantly expressed (Diwan et al., 2004; Parry et al., 1997). At present, it is unclear if TNF is physiologically produced by thymic stromal cells and how the TNF signal is transmitted to differentiating HSPCs. A comprehensive understanding of the physiological signals provided by thymic stromal cells is important to unleash the full potential of *in vitro* T cell development for therapeutic application.

Based on the difference in the developmental origin of thymus-residing DC and B cells, we explored the physiological relevance of human in situ intrathymic DC development and reasoned that this may have unique and additional roles in supporting other stages of human T cell development.

RESULTS

IRF8 expression is driven by Notch signalling and marks T- and DC-lineage priming

Our recent work on single-cell RNA sequencing (scRNA-seq) of *ex vivo* $CD34^+$ postnatal thymocytes identified two distinct TSP subsets (Lavaert et al., 2020). In contrast to the TSP1 that was predicted to be the canonical human T cell precursor, the TSP2 subset was suggested to support both T and DC development, presumably via intrathymic expansion of a hematopoietic progenitor cell (HPC) population (**Figure 1A**). In accordance with the role of IRF8 as a marker for human DC-lineage development (Lee et al., 2017), we observed a gradual increase in *IRF8* expression as the TSP2 is projected to differentiate along the DC-lineage developmental trajectory (**Figure 1B**). Consistent with previous findings that the earliest human and murine thymic progenitors are transcriptionally distinct (Lavaert et al., 2020; Le et al., 2020), we did not detect IRF8 protein in immature murine thymocytes (**Figures S1A-1B**). Thus, expression of IRF8 in early T cell development is a distinct feature in human and we reasoned that further characterization of IRF8 could resolve the intricate developmental relationship of T- and DC-lineages.

To validate the previously annotated immature human thymocyte populations (Lavaert et al., 2020) phenotypically, we divided *ex vivo* $lin^-CD4^-CD34^+$ thymocytes into four subsets based on their expression of IRF8 and CD1a, a marker for human T-lineage commitment (**Figures 1C-1D**) (Blom and Spits, 2006), and further examined the expression of other cell surface and intracellular markers on these subsets (**Figure 1E**). This revealed that the $IRF8^{lo}CD1a^-$ subset corresponds to the previously annotated TSP2 and HPC populations that express high levels of PU.1, characteristic for multipotent HPCs, and, consistent with the scRNA-seq analysis, expresses markers that are representative of both T- (such as GATA3 and cyCD3) and DC- (such as CD44 and CD123) lineages (Lavaert et al., 2020; Marquez et al., 1995; Martin-Gayo et al., 2017; Van de Walle et al., 2016b). On the other hand, the $IRF8^{hi}CD1a^-$ subset that

corresponds to the annotated GMP IRF8^{hi} population only expresses DC lineage markers, whereas the IRF8^{-}CD1a$^{-/+}$ subsets only express T-lineage markers, including CD5, CD127 (also known as IL-7 receptor α chain), GATA3 and cyCD3 (**Figures 1E-1F**). Importantly, overlay of these four subsets of immature thymocytes (**Figure S1C**) revealed that the IRF8^{lo}CD1a^{-} subset co-expresses low levels of the T-lineage transcription factor GATA3 and is thereby positioned at the bifurcation of the T- and DC-lineages (**Figure 1G**). Hence, low expression of IRF8 in these CD34^{hi} immature thymocytes (**Figure 1E**) marks T- and DC-lineage priming rather than specification towards one of these lineage cell fates.

To validate the developmental potential of these subsets, we sorted *ex vivo* lin^{-}CD4^{-}CD34^{+} thymocytes, based on CD123 and CD1a expression (**Figures S1D-S1F**), and co-cultured them on OP9-DLL4 stromal cells to study T-lineage potential and on OP9 stromal cells to track DC development. CD123 is a surrogate marker for intracellular IRF8 expression (Cytlak et al., 2020; Zeng et al., 2019), which was confirmed in our human CD34^{+} thymocytes. Indeed, the sorted CD123^{lo}CD1a^{-} subset has lower levels of IRF8 expression but higher CD34 expression, which matches the profile of the IRF8^{lo}CD1a^{-} subset (**Figure 1E and S1F**). Consistent with its bi-phenotypic profile and higher CD34 expression, the CD123^{lo}(IRF8^{lo})CD1a^{-} subset was found to efficiently and robustly differentiate into both T- (**Figures 1H-1I**: CD7^{+}CD5^{hi} T cell precursors on OP9-DLL4) and DC- (**Figures 1J-1K**: HLA-DR^{+}CD123^{+} plasmacytoid DCs (pDCs) and HLA-DR^{+}CD1c^{+} conventional DCs (cDCs) on OP9) lineages in co-culture assays. The CD123^{hi}(IRF8^{hi})CD1a^{-} subset, which is relatively more mature (**Figure 1E and S1F**), generated only negligible amounts of T cell precursors (**Figures 1H-1I**) and predominantly gave rise to pDCs (**Figures 1J-1K**), consistent with a recent report that showed that the developmental pathway of human pDCs is IRF8^{hi}-dependent whereas the development of cDCs, depending on their subsets, requires low or high levels of IRF8 expression (Cytlak et al., 2020). In contrast, we found that both the CD123^{-}(IRF8^{-})CD1a^{-} and CD123^{-}(IRF8^{-})CD1a^{+}

subsets failed to develop into pDCs and cDCs (**Figures 1J-1K**), in agreement with their reduced CD44 expression (**Figure 1E**). These results are consistent with the progressive T-lineage restriction of thymic precursors as they undergo T-lineage commitment which is marked by the reduction of CD44 and subsequent induction of CD1a expression (Cante-Barrett et al., 2017; Van de Walle et al., 2016b). Overall, our data demonstrates that the bi-phenotypic $CD123^{lo}(IRF8^{lo})CD1a^{-}$ subset, corresponding to the TSP2 and HPC populations, possesses T and DC potential. This common developmental origin of both T cells and DCs was further confirmed through analysis of TCR rearrangements which occur in an ordered manner during T-cell development (Dik et al., 2005). In humans, *Dδ2-Dδ3* rearrangements within the *TCR-δ* locus occur first, already within the $CD34^{+}CD7^{lo}CD5^{-/lo}CD1a^{-}$ thymic progenitors (Cieslak et al., 2014), and we detected comparable frequencies of *Dδ2-Dδ3* rearrangements in the sorted *ex vivo* $CD34^{+}CD123^{lo}(IRF8^{lo})CD1a^{-}$ and $CD34^{+}CD123^{hi}(IRF8^{hi})CD1a^{-}$ subsets as in thymic cDCs and thymic pDCs (**Figure 1L**), confirming that human thymic DCs are derived from a T cell precursor that has already initiated TCR rearrangements and thus received T-lineage inductive signals.

$IRF8^{lo}$-expressing TSP2 and HPC populations also express CD7, a Notch target during early human T cell development (De Smedt et al., 2002; Lavaert et al., 2020). To investigate if Notch signalling is permissive for induction of IRF8 expression during early human T cell development, we exposed human cord blood-derived HSPCs to different human Notch ligands to examine the Notch-dependent induction of IRF8 in TSPs. *IRF8* expression was only upregulated by DLL1-, DLL4- and JAG2-mediated activation of Notch signalling (**Figure 2A**), consistent with the potential of these ligands, but not of JAG1, to induce human T-lineage specification (Jaleco et al., 2001; Van de Walle et al., 2011). Nevertheless, further and sustained expression of IRF8 during intrathymic DC development at later stages could be less Notch-dependent (Martin-Gayo et al., 2017). Similarly, expression of IRF8 protein was induced

significantly in HSPCs that overexpressed constitutively active intracellular Notch1 (ICN1) (**Figures 2B-2C**). Further immunophenotyping revealed that IRF8^{+} ICN1-transduced HSPCs display stronger expression of CD10, which is also expressed by the HPC but not the TSP2 population, and of CD127, the receptor for IL-7 (**Figure 2D**) (Lavaert et al., 2020; Weekx et al., 2000). Although IRF8 expression is promoted by activated Notch signalling in human TSPs, analogous to during murine macrophage development (Xu et al., 2012), IRF8 expression decreases during further differentiation towards ETPs and is silenced in the subsequent T-developmental stages (**Figures 1B-1G**) (Lavaert et al., 2020), a critical event since continuous high level IRF8 expression is inhibitory for the development of CD7^{+}CD5^{hi}CD1a^{+} T-lineage committed precursors (**Figures 2E-2G**). Our previous work identified GATA3 as a driver of human T-lineage commitment that involved restraining of Notch signalling activity (Van de Walle et al., 2016b). Given that IRF8 is positively regulated by Notch signalling (**Figures 2A-2D**) and given that we observed that IRF8 expression decreases with concomitant increased expression of GATA3 (**Figure 2H**), we postulated that silencing of IRF8 expression is mediated by GATA3. Enforced expression of GATA3 in human cord blood-derived HSPCs indeed significantly downregulated endogenous expression of IRF8 at both RNA and protein levels (**Figures 2I-2K**). The effect was reversed in a *GATA3* knockdown setting (**Figure 2L**). Thus, although IRF8 expression is permissive for T-lineage specification even at high levels (**Figures 2E-F**), it is mandatory silenced in physiological conditions by GATA3 to drive T-lineage commitment. Overall, our data indicates that Notch signalling mediates simultaneous T- and DC-lineage priming in human HSPCs via induction of IRF8 expression. However, fine-tuning of IRF8 expression thereafter is critical to discriminate between further T- and DC-lineage development.

Low level IRF8 activity promotes the development of transmembrane TNF-expressing CD7$^+$CD123$^+$ progenitors and of CD7$^+$CD5$^+$ T cell precursors

To examine if low IRF8 expression promotes early T cell development, we transduced HSPCs with an IRF8-ERT2 fusion protein-encoding virus where IRF8 activity is tamoxifen-dependent (**Figure 3A**) (Feil et al., 1997). At day 7 post OP9-DLL4 co-culture, with 50 nM of 4 hydroxytamoxifen (4-OHT) treatment, low dose of active IRF8 increased the generation of CD7$^+$CD5$^+$ T cells precursors (**Figures 3B-3C**). However, with increasing doses of 4-OHT, the promoting effect was gradually lost and a CD34$^+$CD7$^+$CD5$^-$ population with increasing CD123 expression was observed (**Figures 3B, 3D**). Hence, low levels of IRF8 are beneficial for T-lineage development, whereas high levels skew the differentiation of HSPCs to the DC-lineage. To delineate the underlying mechanism, we sorted co-cultured CD7$^+$ cells at day 4 for bulk RNA-seq. Although intracellular expression of IRF8-ERT2 was readily detected post transduction, without 4-OHT treatment, IRF8-ERT2-transduced cells had a similar transcriptome compared to control-transduced cells (**Figures S2A-S2B**). With 50 nM of 4-OHT treatment, genes associated with interferon (IFN) signalling were significantly downregulated (**Figures S2C and 3E**). Given that low dose of active IRF8 promotes the generation of T cell precursors (**Figures 3B-3C**), our data suggests that inhibition of IFN signalling (**Figure 3E**) is important to steer the development of HSPCs along T-lineage. Consistently, using UCell (Andreatta and Carmona, 2021), we found that the IFN-related gene signature derived from our bulk RNA-seq analysis (**Figure 3E**) is highly enriched in the TSPs, but gradually downregulated as they differentiate to become T-lineage specified and committed (**Figures 3F and S2E**). Notch target genes such as *CD3E* and *DTX1* were consistently upregulated, although not statistically significant (**Figure S2D**) (Van de Walle et al., 2016b), but *TNF* was significantly upregulated (**Figure 3E**) and sTNF has been reported to enhance the generation of human T cell precursors (Dos Santos Schiavinato et al., 2016; Edgar et al., 2022;

Moirangthem et al., 2021; Smits et al., 2007; Weekx et al., 2000). Using complementary bulk ATAC-seq, we found that 92% of the significant changes in chromatin accessibility regions of control-transduced T-lineage specified $CD7^+$ versus more immature non-specified $CD34^+CD7^-$ cells were shared by IRF8-ERT2-transduced $CD7^+$ cells that also have far more unique changes (**Figure 3G**). Transcription factor motif analyses showed that those unique chromatin accessibility changes mostly harboured ETS (opened regions) or GATA (closed regions) family binding sites (**Figures S2F-S2G**). IRF8-ERT2-transduced $CD7^+$ cells appeared to develop further along the T-lineage as an enhancer of *CEBPE*, essential for granulocytic differentiation, was significantly closed (**Figure 3H**) (Shyamsunder et al., 2019). In agreement with the increased *TNF* expression (**Figure 3E**), we found significant opening of the *TNF* core promoter in $CD7^+$ cells in the presence of low dose of active IRF8 (**Figure 3H**). TNF signalling is transmitted through cells via activation of TNF receptor 1 (TNFR1) and 2 (TNFR2) that mediate both common but also receptor-specific downstream signalling events (Fischer et al., 2020). To clarify how *TNF* expression promotes the generation of human T cell precursors, we sought to characterize the expression of TNF and TNFR on different subsets of $CD7^+$ cells. Surface expression of TNFR1 was barely detected (**Figures S2H-S2I**). In contrast, $CD7^+CD123^+$ progenitors, whose development is promoted by IRF8 (**Figures 3B, 3D**), co-expressed TNFR2 and tmTNF while $CD7^+CD5^+$ T cell precursors only expressed TNFR2 (**Figures 3I-3J**). Therefore, we speculated that low dose of active IRF8 promotes the development of tmTNF-expressing $CD7^+CD123^+$ progenitors which in turn activate TNF signalling in T cell precursors via TNFR2, thereby indirectly promoting $CD7^+CD5^+$ T cell precursor expansion.

IRF8-dependent DC-biased $CD123^+CD127^+$tmTNF$^+$ progenitors non-cell-autonomously promote the development of human T cell precursors.

Using IRF8-deficient human induced pluripotent stem cells (iPSCs) (Sontag et al., 2017) and the embryonic mesodermal organoid (EMO) system (**Figure 4A**) (Montel-Hagen et al., 2019), we also studied the impact of IRF8 loss on T cell development. While IRF8 is dispensable for the differentiation of iPSCs into embryonic mesodermal progenitors (EMPs) (**Figures S3A-S3B**) and for the development of $CD45^+CD34^+$ hematopoietic progenitors (Sontag et al., 2017), loss of IRF8 also did not affect the development of $CD7^+CD5^+$ T cell precursors, nor of $CD4^+CD8b^+$ double positive (DP) thymocytes (**Figures 4B-4C**), further supporting the hypothesis that IRF8 might indirectly promote early T cell development. This is not surprising because human thymopoiesis is predicted to be mainly sustained by the TSP1 subset that does not express IRF8 (**Figures 1A-1B**) (Lavaert et al., 2020). In support of this hypothesis, immunophenotyping immediately after the hematopoietic induction phase, prior to inducing T-lineage differentiation (**Figure 4D**), revealed that IRF8 loss severely impaired the development of a subset of HPCs that co-express CD123 and CD127 (**Figures 4E-4F**) and that originates exclusively from hematopoietic progenitors that express TNFR2 (**Figure 4E and S3C**). Furthermore, we confirmed that this subset expresses IRF8 and, importantly, specifically tmTNF (**Figure 4G).** The few remaining $CD123^+CD127^+$ HPCs in the *IRF8*$^{-/-}$ EMOs displayed impaired tmTNF expression **(Figures 4H-4I).** Although cleavage of tmTNF could give rise to sTNF (Black et al., 1997), we did not detect sTNF in the EMO cultures (**Figures S3D-S3F**) (Black et al., 1997) and conditioned medium from the control-EMOs could not rescue the development of $CD123^+CD127^+$ precursors from *IRF8*$^{-/-}$ EMPs (**Figures S3G-S3H**). We sorted this subset, without staining of CD127 to avoid blockade of its function during development (Weekx et al., 2000), for limiting dilution co-culture analysis (**Figure 4D**). Despite being cultured in conditions that support T cell development, these progenitors are DC-biased and have limited T cell potential (**Figures 4J-4K**). To investigate if these IRF8-dependent $CD123^+CD127^+tmTNF^+$ progenitors ($HLA\text{-}A2^+$) indeed can promote T-cell precursor

generation from HSPCs (HLA-A2$^-$) in a cell non-autonomous manner, we sorted them as described earlier to spike the artificial thymic organoid (ATO) system (**Figure 4L**) (Seet et al., 2017). Compared to the control, HSPCs gave rise to more T cell precursors in the presence of tmTNF-expressing CD123$^+$CD127$^+$ precursors (**Figures 4M-4N, S3I-S3L**) and these T cell precursors are relatively more mature as evidenced by the expression of CD1a (**Figure 4O**) (Van de Walle et al., 2016b). Collectively, our data show that IRF8 promotes the generation of human T cell precursors indirectly via cellular crosstalk and through the development of DC-biased CD123$^+$CD127$^+$ progenitors that express tmTNF.

TNFR2 is expressed during human T-lineage specification and is associated with reduced myeloid potential

Consistent with the findings derived from experiments using IRF8-ERT2-transduced HSPCs (**Figures 3I-3J**) and IRF8-deficient iPSCs (**Figures 4E-4I**), we confirmed that tmTNF is expressed by the TSP2 and HPC-annotated *ex vivo* immature thymocyte populations (**Figure 5A**: CD7$^+$CD123^{lo}(IRF8^{lo})CD1a$^-$ subset 2) at the highest level (**Figure 5B, S4A**). Compared to the TSP2s and HPCs, ETP and T-lineage specified immature thymocytes (**Figure 5A**: CD7$^+$CD123$^-$CD1a$^-$ subset 4) had similar expression levels of TNFR2 and CD127 but lower level of tmTNF (**Figure 5B, S4A**). The T-lineage committed immature thymocytes (**Figure 5A**: CD1a$^+$ subset 5) had the lowest level of tmTNF but the highest level of CD127 (**Figure 5B, S4A**). Since TNF signalling can be modulated by changes in expression of TNFR1 and TNFR2 during human aging (Aggarwal et al., 1999), we used the ATO system (Seet et al., 2017) to characterize the kinetic expression of both TNF receptors during early T cell development on differentiating HSPCs that were derived from three human ontogenetic stages. At day 2 of culture, only cord blood-derived HSPCs expressed detectable amounts of TNFR1 (**Figure S4B**) but this was gradually downregulated during further culture as these HSPCs

differentiated along the T-cell lineage (**Figure S4B**). TNFR1 expression was also hardly detected on the differentiating HSPCs in OP9-DLL4 co-culture assay (**Figures S2H-S2I**) and on the *ex vivo* immature thymocytes (**Figure 5B**). In contrast, TNFR2 expression is induced or maintained, dependent on the source of HSPCs (**Figures S4C-S4D**), and transiently co-expressed with CD7 expression which is driven by Notch signalling (**Figures 5C-5D**) (De Smedt et al., 2002). This indicates that TNF signalling is mediated by TNFR2 instead of TNFR1 activation during early human T cell development and may explain the faster and more efficient development of T cells from fetal compared to adult sources of HSPCs (De Smedt et al., 2011; Offner et al., 1999; Patel et al., 2009). Detection of CD5 expression on TNFR2^{+}CD7^{+} cells confirmed their T-lineage identity (**Figure 5E**) which was further corroborated by the observation that the development of TNFR2^{+}CD7^{+} cells was impaired in ATO cultures without IL-7 supplementation (**Figures 5F-5G**), resulting in expression of CD123 instead of CD5 (**Figures 5H**). Given that CD7 expression on hematopoietic progenitors marks loss of myeloid and erythroid potential (Hao et al., 2001; Hoebeke et al., 2007), our data suggests that such lineage restriction may occur earlier since TNFR2 expression precedes CD7 induction. Indeed, in an ATO system spiked with MS5 stromal cells that express both human DLL4 and human tmTNF (MS5-DLL4/tmTNF) (**Figure S5**), we discovered that TNFR2^{+} HSPCs have higher T cell potential compared to TNFR2^{-} HSPCs (**Figures 5I-K**). However, TNFR2^{+} HSPCs have reduced myeloid potential (**Figures 5L-5M**).

Selective targeting of TNFR2 enhances generation of human T cell precursors

Given that TNFR2 is induced during T-lineage specification (**Figure 5**) and robust activation of TNFR2 requires the binding of tmTNF instead of sTNF (Grell et al., 1995; Grell et al., 1998), we sought to recapitulate activation of TNF signalling via TNFR2 in order to maximize the generation of human T cell precursors *in vitro*. To achieve this, we used the generated MS5-

DLL4/tmTNF stromal cells (**Figure S5**) to mimic the physiological tmTNF signal provided by $CD123^+CD127^+$ DC-biased progenitors (**Figures 3I-3J, 4E-4I, 5A-5B**) in the conventional ATO system (Seet et al., 2017). Importantly, unlike sTNF, tmTNF can activate both TNFR1 and TNFR2 upon binding (Grell et al., 1995; Grell et al., 1998). We rationalized that a low-density tmTNF signal would be necessary to allow preferential targeting of TNFR2 on differentiating HSPCs while minimizing activation of TNFR1 which is normally downregulated during T-lineage development (**Figures S2H-S2I, 5B, S4A**). Therefore, we assembled ATOs using a combination of MS5-DLL4/tmTNF cells and MS5-DLL4 cells at different ratios and examined its impact on the generation of human $CD7^+CD5^+$ T cell precursors (**Figure 6A**). At day 10 post culture, the presence of tmTNF signal, presented by 1 to 100% of the total MS5 cells in an ATO, did not affect the cellular output compared to the control (**Figure 6B**). However, the presence of tmTNF signal, regardless of its density increased the frequency and yield of T cell precursors. More strikingly, a significant linear trend of an inverse correlation between the density of the tmTNF signal and the cellular pool of undifferentiated $CD34^+$ HSPCs was found (**Figures 6C-6E**). The low density of tmTNF signal, at 1 %, led to an expansion of T cell precursors without skewing differentiation of HSPCs over proliferation. Furthermore, when tmTNF is presented by 1 % of the total stromal cells in an ATO, the generated CD1a-expressing T cell precursors display the lowest expression of HLA-DR, similar to the control (**Figures 6F-6G**). This is physiologically relevant and significant because *ex vivo* T-lineage committed $CD1a^+$ immature thymocytes have minimal expression of HLA-DR at RNA and protein levels (**Figures 1E-1F**) (Van de Walle et al., 2016b). Since upregulation of HLA-DR is a unique feature of activated TNFR1-specific signalling (Maney et al., 2014), this demonstrates that *in vitro* recapitulation of tmTNF signal, at 1 % density, selectively targets TNFR2 and maximizes the generation of T cell precursors per HSPCs. The promoting effect of TNFR2 activation on early T cell development was further validated as the

frequency and yield of T cell precursors increased with supplementation of EHD2-scTNF$_{R2}$ (Dong et al., 2016), a TNF mutein and a TNFR2-selective agonist, to the ATO cultures (**Figures 6H-6I, S6**).

sTNF mediates TNFR1-specific signalling in a dose-dependent manner and accelerates T-lineage differentiation of HSPCs at the expense of their maintenance

While sTNF has been used to enhance the generation of human T cell precursors (Dos Santos Schiavinato et al., 2016; Edgar et al., 2022; Moirangthem et al., 2021; Smits et al., 2007), our data indicates that tmTNF, instead of sTNF, mediates TNF signalling *in vivo* in developing T cells via activation of TNFR2. Since previous studies have shown that the sTNF/TNFR1 axis regulates the fate of human HSPCs by promoting their differentiation but not their self- renewal (Dybedal et al., 2001; Senyuk et al., 2018), we speculated that the reported promoting effect of sTNF on the generation of human T cell precursors results from the accelerated differentiation of HSPCs at the expense of their maintenance. To re-examine this, we used the ATO system where T cell development is supported by a minimum number of cytokines at the minimal concentration (1L-7 and FMS-like tyrosine kinase 3 ligand at 5 ng/mL) (**Figure S76A**) (Seet et al., 2017). This allowed us to determine the true effect of sTNF on the generation of human T cell precursors without interference from cytokines such as stem cell factor and thrombopoietin that are known to stimulate HSPC proliferation and that are used in other *in vitro* systems (Dos Santos Schiavinato et al., 2016; Edgar et al., 2022; Moirangthem et al., 2021; Smits et al., 2007; Zielske and Braun, 2004). After 10 days of culture, we observed that sTNF at 0.25, 5 and 100 ng/mL did not improve the total ATO cell yield (**Figure S76B**). In fact, high dose of sTNF (100 ng/mL) significantly decreased the total cell yield compared to the untreated control (**Figure S76B**). Further examination of the cellular composition of ATOs revealed that, compared to the control, increasing dosage of sTNF treatment is linearly correlated with the depletion of

undifferentiated $CD34^+$ HSPCs but is inversely correlated with the yield of $CD7^+CD5^+$ T cell precursors (**Figures S76C-S76E**). Only sTNF treatment at the lowest tested dose (0.25 ng/mL) significantly increases the generation of T cell precursors because the pool of $CD34^+$ HSPCs was significantly depleted but to the least extent compared to sTNF treatment at higher dose. Overall, this indicates that, in the presence of Notch signalling, HSPCs are steered by sTNF in a dose-dependent manner to favour T-lineage differentiation instead of proliferation. The previously reported positive effect of sTNF on the expansion of human T cell precursors at high dosages was inadvertently contributed by the activity of the other cytokines that counteract the HSPC-depleting effect of sTNF and that were used in the assayed systems (Dos Santos Schiavinato et al., 2016; Edgar et al., 2022; Moirangthem et al., 2021; Smits et al., 2007). Furthermore, sTNF dose-dependently increased the aberrant expression of HLA-DR in CD1a-expressing T-lineage committed precursors (**Figures S76F-S76G**), which physiologically have minimal expression of this marker (**Figures 1E-1F**) (Van de Walle et al., 2016b). Since increased expression of HLA-DR during the maturation of human dendritic cells was shown to be a unique feature of activated TNFR1-specific signalling (Maney et al., 2014), and since activation of TNFR1 and TNFR2 can induce both common and receptor-specific downstream signalling (Fischer et al., 2020), our data suggests that sTNF at low dose increases the generation of T cell precursors by circumventing the activation of TNFR1-specific downstream signalling that could lead to aberrant HLA-DR expression and depletion of HSPCs but retaining the activation of common TNF downstream signalling that promotes early T cell development in the human.

TNF-activated lymphoid progenitors downregulate expression of interferon-related genes and are competent in T-lineage development at late stages.

To get a better understanding of how TNF signalling promotes early T cell development physiologically via the tmTNF/TNFR2 axis through cellular crosstalk, and in comparison to the experimental setting in which the TNFR1 axis is activated by the very low dose of sTNF, we used single-cell RNA sequencing (scRNA-seq) to unravel the global impact of TNF signalling on HSPCs being differentiated in the ATO system (Seet et al., 2017) (**Figure 7A**). Following quality control and dimensionality reduction analyses, 26 distinct clusters were identified (**Figure 7B**: labelled 0 to 25), containing cells derived from all conditions (**Figure S87A**) and at different cell cycle phases (**Figures S87B**). Annotation of these clusters based on cell-type specific gene markers allowed us to depict the heterogeneity that is present within the differentiating HSPCs despite that they were cultured in T-stimulating conditions (**Figure 7C**). Nevertheless, clusters that annotated as T progenitors and that express T-lineage specific marker genes such as *RAG2*, *CD1E* and *BCL11B* comprised the biggest population among the differentiating cells (**Figures 7C-7D**) (Lavaert et al., 2020). Consistent with the promoting effect of TNF signalling on early T cell development, 45.6% and 41.5% of the cells labelled as T progenitors were derived from sTNF-treated and tmTNF-spiked ATOs, respectively (**Figure 7D**). Interestingly, scRNA-seq analyses also identified that sTNF and tmTNF have differential impacts on the development of other minor hematopoietic populations. For example, 62.3 % of the cells labelled as macrophages were derived from sTNF-treated ATOs whereas 69.5 % of the cells labelled as mast cells were derived from tmTNF-spiked ATOs (**Figure 7D**). This suggests that TNF signalling, when mediated by the sTNF/TNFR1or the tmTNF/TNFR2 axes, is indeed not identical in differentiating HSPCs and results in receptor-specific downstream signalling. In accordance with the UCell analysis on *ex vivo* $CD34^+$ thymocytes (**Figures 3G, S2E**) and our recent scRNA-seq analysis that predicted a role for interferon signalling in the intrathymic DC-lineage developmental trajectory (Lavaert et al., 2020), we found that the interferon-related gene signature was highly enriched in the lymphoid progenitors and in the

DC populations compared to in the T progenitors (**Figure 7E, S87C**). It is noteworthy that more than 70% of the lymphoid progenitors were derived from the control as T-lineage specification is promoted within the TNF-activated ATOs (**Figure S87D**). Further analysis revealed that, in contrast to the control, the expression of these interferon-related genes was downregulated in lymphoid progenitors derived from the TNF-activated ATOs (**Figure 7F**). Physiologically, the expression of these genes was gradually downregulated as TSPs differentiate along the T-lineage (**Figure 3G, S2E, S87E**) but was highly enriched in intrathymic DC intermediate populations (Lavaert et al., 2020). Furthermore, activated TNF signalling was shown to block the *in vitro* differentiation of pDCs from human immobilised HSPCs (Palucka et al., 2005). Hence, our data demonstrates that, in the presence of Notch signalling, activated TNF signalling helps to steer HSPCs towards T-lineage differentiation by inhibiting IFN signalling that would otherwise support DC-lineage development. However, a recent study reported that continuous exposure of HSPCs to sTNF inhibits the development of DP T cells (Edgar et al., 2022). To investigate if physiological tmTNF/TNFR2 stimulation results in the generation of T cell precursors with enhanced T cell maturation potential compared to sTNF/TNFR1 activated cells, we sorted TNF stimulated $CD7^+$ progenitors for further culture (**Figure 7G**). In the absence of further TNF stimulus, sTNF-activated $CD7^+$ progenitors displayed lower potential to develop into DP T cells compared to the control (**Figures 7H-7I, S8F-S8G**) although they had significantly higher outputs of $CD3^+TCR\alpha\beta^+$ and $CD3^+TCR\gamma\delta^+$ T cells (**Figures 7J-7L, S8H-S8K**). In contrast, $CD7^+$ progenitors derived from tmTNF-spiked ATOs gave higher outputs of T cells at all the late stages being examined (**Figures 7H-7L, S8F-S8K**). Hence, *in vitro* recapitulation of physiological tmTNF/TNFR2 signalling generates more T cell precursors (**Figures 6E, S76E**) that are also of better quality compared to when only TNFR1 is activated through sTNF, and this has important implication for unleashing the full potential of *in vitro* T cell development for therapeutic application.

DISCUSSION

Our study unravels the physiological significance of intrathymic DC development in supporting early human T cell development, thereby clarifying their in situ development in the thymus from TSPs, in contrast to B cells that only have a supportive role as mature cells in the late stages of T cell development. Although previous studies in the human thymus revealed in situ development of DCs, it was unclear if thymic DCs develop in a distinct, non T-lineage supporting thymic niche from multipotent TSPs in which T-lineage differentiation has not yet been initiated (Martin-Gayo et al., 2017) or whether they can share an early developmental program with T cells (Lavaert et al., 2020; Le et al., 2020). Our work now demonstrates that the DC- and T-lineages are concurrently primed in the TSPs that express low levels of IRF8. Consistent with the presence of $CD34^{+}IRF8^{hi}$ DC precursors and mature pDCs and cDCs in the thymus that display *TCRD* gene rearrangements, we show that the recently identified TSP2- and HPC-annotated $CD34^{+}CD123^{lo}IRF8^{lo}$ human thymocytes are bi-phenotypic, have initiated *TCRD* rearrangements and have the potential to develop into T- and DC-lineage cells (Lavaert et al., 2020). Physiologically, we found that IRF8 expression in human HSPCs is upregulated following Notch signalling but only via Notch ligands (DLL1, DLL4 and JAG2) that are capable of inducing human T-lineage specification (Jaleco et al., 2001; Van de Walle et al., 2011). Furthermore, although IRF8 was reported as a marker for human DC lineage specification (Lee et al., 2017), we found that enforced expression of IRF8 in human HSPCs is permissive for T-lineage specification. Overall, our study indicates that activation of Notch signalling in human TSPs not only induces T cell development but also allows supporting DC-lineage differentiation via the induction of IRF8 expression.

Importantly, DLL1-dependent Notch signalling has been shown to be critical to promote *in vitro* differentiation of cDCs from both mouse and human hematopoietic progenitors (Balan et al., 2018; Kirkling et al., 2018). However, single-cell analysis of the earliest CD117-expressing

murine thymic progenitors did not uncover a developmental trajectory of DC-lineage cells (Le et al., 2020; Zhou et al., 2019). Although thymic DCs do exist in the murine thymus, they appear to be derived from $CD117^-$ thymic progenitors that do not sustain T cell development at physiological steady state (Benz et al., 2008; Luche et al., 2011; Moore et al., 2012; Porritt et al., 2004). Thus, murine thymic DCs seem to have a separate developmental origin compared to T cells and we also did not detect IRF8 protein in these CD117-expressing immature mouse thymocytes. The rationale for this absence of IRF8 expression and of the correlated developmental trajectory of the DC-lineage from the murine counterparts of human $CD34^+$ thymocytes is unclear. Nevertheless, this further highlights that the downstream Notch network during early T cell development is different in human compared to in mice, in addition to the known differences in Notch activation status (Taghon et al., 2012). Physiologically, we found that IRF8 expression is silenced by GATA3, a key transcriptional regulator during T cell development that restrains Notch signalling in order to induce human T-lineage commitment (Van de Walle et al., 2016b). Hence, the unique expression of IRF8 during early human T cell development might necessitate and explain the earlier peak in the kinetic expression profile of *GATA3* compared to other critical T-lineage transcription factors such as *TCF7* and *BCL11B* during the ETP and specification stages of human T cell development and this results in altered dynamics of the activity of these factors compared to what has been described in mice (Lavaert et al., 2020; Rothenberg, 2021; Van de Walle et al., 2016b; Weber et al., 2011).

To date, thymus-residing human DCs have only been described to support thymocyte selection and maturation (Martin-Gayo et al., 2010; Park et al., 2020; Watanabe et al., 2005). Our work now demonstrates that intrathymic DC progenitors (TSP2 and HPC-annotated $CD34^+$ thymocytes) have an early role in promoting human T-lineage specification. Consistent with IRF8 expression being linked to the intrathymic DC potential of human T cell precursors, we could genetically demonstrate that the development of $CD123^+CD127^+$ DC-biased progenitors

and their expression of tmTNF are indeed IRF8-dependent. Our work also reveals that these DC-biased progenitors and T cell precursors arise from differentiating human HSPCs that express TNFR2 in a Notch-stimulating microenvironment, thereby further consolidating that intrathymic DC and T cells share a common developmental origin. However, T cell precursors that are IRF8-independent do not express tmTNF and their expansion via TNFR2 activation is instead mediated by cellular cross-talking with tmTNF-expressing DC-biased progenitors. Importantly, we clarify that tmTNF, instead of sTNF, is the physiological thymic signal that leads to activation of TNF signalling via TNFR2, instead of TNFR1, to ensure generation of developmentally competent human T cell precursors. Previous studies reported that sTNF enhances the generation of human T cell precursors *in vitro* (Dos Santos Schiavinato et al., 2016; Edgar et al., 2022; Moirangthem et al., 2021; Smits et al., 2007; Weekx et al., 2000). However, we found that sTNF activates TNFR1-specific downstream signalling and leads to exhaustion of HSPCs and accelerated differentiation into T-lineage committed human precursors that display aberrant induction of HLA-DR expression (Dybedal et al., 2001; Maney et al., 2014; Senyuk et al., 2018). Although sTNF has been suggested to promote human early T cell development *in vitro* through activation of the downstream NF-κB pathway (Moirangthem et al., 2021), we speculate that this common pathway is instead physiologically mediated by TNFR2 on differentiating TSPs upon crosstalk with tmTNF-expressing DC progenitors (Fischer et al., 2020). We show that although sTNF/TNFR1 activation could partially mimic the physiological tmTNF/TNFR2 axis in promoting early T cell development, which may involve suppression of interferon signalling, TNFR2-specific downstream signalling events could be important to ensure that the generated T cell precursors are developmentally competent. Intriguingly, TNFR2 is known to uniquely mediate the PI3K/AKT/mTOR pathway which has been implicated in the development of DP thymocytes (Swat et al., 2006; Xue et al., 2008) and the pathogenesis of T cell acute lymphoblastic

leukaemia (Fischer et al., 2020; Silva et al., 2008). Hence, further delineation of the downstream pathways of TNFR2-mediated physiological TNF signalling that are involved in the development of human T cell precursors by multi-omics approaches could improve our understanding of their malignant transformation during leukemogenesis.

Last but not least, we demonstrated that selective targeting of TNFR2, by presenting tmTNF at low density or by using a TNFR2-specific agonist, enhances the generation of human T cell precursors. This provides a proof-of-concept to apply selective targeting of TNFR2 to maximize the *in vitro* generation of bona fide human T cell precursors for clinical applications such as immune reconstitution and immunotherapy against cancer. Currently, TNFR2 agonists have been in active development with the aim to treat inflammatory and autoimmune diseases (Fischer et al., 2020). Future study is warranted to explore the possibility of repurposing these agonists to unleash the full potential of *in vitro* T cell development for therapeutic purpose.

ACKNOWLEDGMENTS

We thank C. de Bock (KU Leuven) for the ATAC-seq protocol, J. C. Zúñiga-Pflücker (University of Toronto) for OP9-DLL4-7FS stromal cell line, K. Francois and G. Van Nooten (Department of Human Structure and Repair, Ghent University Hospital) for thymus tissue, the Red Cross Flanders and the Ghent University Hospital Hematopoietic Biobank for cord blood and buffy coat, M. Guilliams (VIB, Ghent University) for an aliquot of IRF8 antibody, K. Weening and A. Kuchmiy (Ghent University) for assistance with molecular cloning, S. Vermaut and K. Reynvoet (Ghent University) for assistance with flow cytometry and cell sorting, F. Branco Madeira (Ghent University) for C57/BL6 mice, M. De Smedt and Jean Plum (Ghent University) for assistance in processing and collection of human tissue, E. De Meester (NXTGNT, Ghent University) for assistance in preparation of samples for scRNA-seq, and R. Colman (Ghent University) for assistance with statistical analyses. This work was supported by the Fund for Scientific Research Flanders (FWO, grants G053816N and G053916N), The Concerted Research Action from the Ghent University Research Fund (GOA, BOF18-GOA-024), The Foundation against Cancer (Stichting Tegen Kanker, 2016-094 and 2020-114), the Chan Zuckerberg Initiative (CZF2019-002445). The computational resources and services used in this work were provided by the VSC (Flemish Supercomputer Center), funded by the Research Foundation - Flanders (FWO) and the Flemish Government – department EWI. Research reported in this publication was performed at the CORE Flow Cytometry and NXTGNT sequencing facilities of Ghent University, Belgium.

AUTHOR CONTRIBUTIONS

K.L.L. conceived the study, designed and performed experiments, analysed data and wrote the manuscript. J.R. analysed bulk ATAC-seq data. M.L. and T.P. analysed the previously

published scRNA-seq data. T.P. and L.B. analysed the scRNA-seq data generated in this study. L.T. analysed bulk RNA-seq data. I.V. assisted to set up experiments. I.V.W. performed an experiment related to regulation of *IRF8* expression. J.V., B.V., G.L., P.V.V. and C.L. provided reagents. F.V.N provided expertise in ATAC- and RNA-seq. V.P., R.F., R.E.K. and K.P. provided TNFR2-selective TNF mutein (EHD2-scTNF$_{R2}$). G.D. provided *IRF8*-related constructs. S.S. and M.Z. provided *IRF8*$^{+/+}$ and *IRF8*$^{-/-}$ iPSCs. T.T. supervised the study, designed experiments, and wrote the manuscript. All authors have seen, reviewed and approved the final version of the manuscript.

DECLARATION OF INTERESTS

K.L.L. and T.T. have filed a PCT application (PCT/EP2022/063712: Generating T cell precursors via agonizing tumour necrosis factor receptor 2) with the European Patent Office on 20th May 2022.

METHODS

Maintenance of cell lines

OP9 stromal cells that express GFP only (control) and different human Notch ligands were generated and cultured as described previously (Dolens et al., 2016; Van de Walle et al., 2011). Jurkat and HL-60 cell lines (ATCC) were cultured as described previously (Dolens et al., 2020; Taghon et al., 2001). OP9-DLL4-7FS stromal cells (Zúñiga-Pflücker lab (Chen et al., 2021)) that express human Interleukin-7 (IL-7), stem cell factor (SCF) and FMS like tyrosine kinase 3 ligand (FLT3-L) were cultured in MEMα medium containing 5 % fetal calf serum, 100 units/mL penicillin, 100 µg/mL streptomycin and 2 mM L-glutamine. MS5 (Itoh et al., 1989; Taghon et al., 2002), previously generated MS5-DLL4 (Dolens et al., 2020)) and MS5-DLL4/tmTNF (generated herein) stromal cells were cultured in MEMα medium containing 10 % fetal calf serum, 100 units/mL penicillin and 100 µg/mL streptomycin. *IRF8*$^{+/+}$ and *IRF8*$^{-/-}$ human induced pluripotent stem cells (iPSCs) are from Zenke lab (corresponding to iPS2) and cultured as described previously (Sontag et al., 2017). All cell lines were periodically checked for mycoplasma contamination.

Isolation of human hematopoietic and thymic progenitors

Postnatal thymus was obtained from patients undergoing cardiac surgery with informed consent of parents or guardians. Umbilical cord blood and adult buffy coats were also obtained with informed consent of donors. Fetal liver was obtained from legally interrupted pregnancies with informed consent of the parents. All human cells and tissues were used with permission of and according to the guidelines of the Medical Ethical Commission of Ghent University Hospital, Belgium. Mononuclear cells from thymic total cell suspension, cord blood and buffy coats were isolated by Lymphoprep density gradient centrifugation (Axis-Shield, cat. 1114547) (Van de

590 Walle et al., 2016a). Subsequently, $CD34^+$ cells were enriched by magnetic-activated cell
591 sorting (Miltenyi Biotec, cat. 130-046-703). Further processing of CD34-enriched cells for
592 downstream experiments is described in the relevant methods. Fetal liver cells, after thawing,
593 were labelled directly with fluorochrome-conjugated antibodies for sorting without CD34
594 enrichment.

595

596 **Isolation of murine thymocytes**

597 Whole thymi were isolated from 5 weeks old C57BL/6 mice that had been euthanized with
598 approval of and according to the guidelines of the Medical Ethical Commission of Ghent
599 University Hospital on animal welfare, and grinded directly onto a pre-wet cell strainer to
600 generate single cell suspension. CD8β-expressing thymocytes were labelled (clone H35-17.2)
601 and depleted using anti-PE microbeads (Miltenyi Biotec, cat. 130-048-101). CD8β-depleted
602 thymocytes were used for surface and intracellular flow cytometric staining.

603

604 **Isolation of human immune cells**

605 To isolate thymic conventional (cDC) and plasmacytoid (pDC) dendritic cells, two rounds of
606 negative selection were performed on mononuclear cells derived from thymic total cell
607 suspension. Cells were first stained with unconjugated anti-CD3 (clone OKT3) and anti-CD8a
608 (clone OKT8) antibodies, and depleted by using Dynabeads Sheep anti-Mouse IgG (Thermo
609 Fisher Scientific, cat. 11031). Subsequently, cells that express different lineage markers (lin:
610 CD3 (clone UCHT1), CD14 (clone M5E2), CD19 (clone HIB19) and CD56 (clone 5.1H11)) or
611 CD34 (clone 581) were also labeled and depleted by using anti-PE microbeads (Miltenyi
612 Biotec, cat. 130-048-101). Finally, the remaining cells were stained with antibodies against
613 CD45 (clone 5B1), CD123 (clone 6H6), CD1c (clone L161) and HLA-DR (clone LN3) to allow

sorting of cDCs (lin$^-$CD34$^-$CD45$^+$HLA-DR$^+$CD123$^-$CD1c$^+$) and pDCs (lin$^-$CD34$^-$CD45$^+$HLA-DR$^+$CD123$^+$CD1c$^-$). To isolate CD19$^+$ B cells and CD3$^+$TCRαβ$^+$ T cells, cord blood-derived mononuclear cells were stained with antibodies against CD19 (clone HIB19), CD3 (clone UCHT1) and TCRαβ (clone BW242/412). Human FcR blocking reagent (Miltenyi Biotec, cat. 130-059-901) was used in all the staining to minimize non-specific binding of antibodies.

Visualization of previously published scRNA-seq data

The *ex vivo* human CD34$^+$ thymocyte scRNA-seq dataset was generated previously (Lavaert et al., 2020). To visualize the expression of *IRF8* and *IL3RA*, violin plots of log2-transformed scRNA-seq count data were generated using the ggplot2 library in R. Heatmaps visualizing pseudobulk scRNAseq count data were generated by summing the counts for individual cells within an annotated population using the sumCountsAcrossCells function from the Scater library (McCarthy et al., 2017). Subsequently, size factors were calculated using the DESeq2 library (Love et al., 2014) and biological replicates were averaged. Finally, the data was scaled using the scale_minmax function from the dynutils library and visualized using the pheatmap library where genes were clustered by using the Ward.D2 algorithm. UCell (Andreatta and Carmona, 2021) was used to score the interferon-related gene signature which was derived from the bulk RNA-seq data analysis. The average expression values for the interferon-related genes were calculated using the AverageExpression function from the Seurat library (Hao et al., 2021) and visualized in a heatmap that was constructed using the pheatmap library in R.

Surface and intracellular flow cytometric staining

To immunophenotype *ex vivo* human thymic progenitors, CD34-enriched cells were first stained with antibodies against lineage markers (lin: as defined above), CD4 (clone M-T466),

CD34 (clone 581) and CD1a (clone HI149). Subsequently, dead cells were labeled by fixable viability dye eFluor506 (Thermo Fisher Scientific, cat. 65-0866-18). Surface-stained cells were then fixed and permeabilized using Foxp3 Transcription Factor Staining Buffer Set (Thermo Fisher Scientific, cat. 00-5523-00) in order to allow intracellular staining of IRF8 (clone V3GYWCH). Antibodies against the tested surface (CD5 (clone UCHT2), CD7 (clone M-T701), CD44 (clone IM7), CD117 (clone 104D2), CD123 (clone 6H6), CD127 (MB15-18C9), CD135 (clone BV10A4H2) and HLA-DR (clone LN3)) and intracellular (cyCD3 (clone UCHT1), GATA3 (REA174) and PU.1 (clone 7C6B05)) markers were fit into the existing staining panel, individually or in combination, depending on the fluorochrome compatibility. Human FcR blocking reagent (Miltenyi Biotec) was included in the staining. Tandem signal enhancer (Miltenyi Biotec, cat. 130-099-887) was used to brighten up intracellular signals.

To immunophenotype *ex vivo* murine immature thymocyte, CD8β-depleted thymocytes were stained with antibodies against markers of different lineages (lin: CD122 (clone TM-β1), CD19 (clone 1D3), NK1.1 (clone PK136), CD11b (clone M1/70), F4/80 (clone BM8), TCRγδ (clone 13D5), Gr-1 (clone RB6), TER119 (clone TER119), CD3e (clone 145-2C11), CD8a (clone 53-6.7) and CD11c (clone N418). Antibodies against c-Kit (clone 2B8), CD25 (clone PC61) and CD44 (clone IM7) were included in the surface staining panel to label different subsets of thymic progenitors (ETP: $lin^{-}CD44^{+}c\text{-}Kit^{hi}CD25^{-}$; DN1 25_{lo}: $lin^{-}CD44^{+}c\text{-}Kit^{hi}CD25^{lo}$; DN2a: $lin^{-}CD44^{+}c\text{-}Kit^{hi}CD25^{hi}$ and DN2b: $lin^{-}CD44^{+}c\text{-}Kit^{lo}CD25^{hi}$) (Yui et al., 2010). Dead cells were labelled as described above. The surface-stained cells were then fixed and permeabilized as described above in order to allow intracellular staining of IRF8 (clone V3GYWCH) and GATA3 (REA174). Mouse FcR blocking reagent (Miltenyi Biotec, cat. 130-092-575) was used throughout the staining.

Other experiments that involved detection of intracellular markers were performed using similar steps. For analyses that involved cell surface staining only, dead cells were labelled by

propidium iodide (Thermo Fisher Scientific, cat. P3566). For analyses of cells harvested from co-culture experiments, both human and mouse FcR blocking reagents (Miltenyi Biotec) were used. Precision Count Beads (BioLegend, cat. 424902) were used where applicable to obtain an absolute cellular count.

Viral constructs and transduction

LZRS-IRES-EGFP (empty vector), LZRS-GATA3-IRES-EGFP, LZRS-ICN1-IRES-EGFP, pLKO.1-EGFP (empty vector), pLKO.1-GATA3 shRNA-EGFP and LZRS-DLL4-IRES-EGFP were constructed and described previously (De Smedt et al., 2002; Taghon et al., 2001; Van de Walle et al., 2009; Van de Walle et al., 2016b). To generate LZRS-IRF8-IRES-EGFP, the *IRF8* insert was released from pIRES2-EGFP-IRF8 by BglII-EcoRI digestion and ligated into the empty vector with BamHI site being destroyed (Mace et al., 2017). To generate LZRS-IRF8-ERT2-P2A-EGFP, *IRF8* was first PCR-amplified from pIRES2-EGFP-IRF8 with the addition of 5'-BglII and 3'-XhoI sites, and the omission of stop codon. Subsequently, the PCR-amplified IRF8 insert was ligated into BamHI- and XhoI-digested LZRS-ERT2-P2A-EGFP (courtesy of Karin Weening, Ghent University where the IRES-EGFP sequence in the empty vector was replaced by ERT2-P2A-EGFP sequence using the GeneART Strings DNA fragment from Thermo Fisher Scientific). To generate LZRS-TNF-IRES-BFP, human *TNF* sequence (NM_000594.4: 178-879 bp) was released from the customized gBlock gene fragment from IDT by BamHI-EcoRI digestion and ligated into LZRS-IRES-BFP. *IRF8* and *TNF* sequences in the newly generated constructs was validated by Sanger sequencing (Eurofins Genomics). Cell culture supernatants containing retro- (LZRS vectors) and lenti- (pLKO.1 vectors) viral particles were generated and used for transduction as described previously (Taghon et al., 2001; Van de Walle et al., 2016b). Cord blood-derived CD34-enriched cells were pre-stimulated with SCF (100 ng/mL), thrombopoietin (TPO: 20 ng/mL) and FLT3-L (100 ng/mL) for 2 days prior

transduction with the use of RetroNectin reagent (Takara Bio, cat. T100B). Spinfection was performed at 890 x g for 90 minutes at 32 ˚C. At day 2 post transduction, cells were stained with antibodies against lineage markers (lin: as defined above) and CD34 (clone 581). $lin^-CD34^+GFP^+$ transduced hematopoietic stem and progenitor cells (HSPCs) were sorted for immediate analysis or for downstream experiments. For experiments that involved IRF8-related constructs, the transduced HSPCs were also stained with antibody against CD123 (clone 6H6) and sorted for $CD123^-lin^-CD34^+GFP^+$. To generate MS5-DLL4/tmTNF stromal cells, MS5 cells were transduced with *DLL4* (*EGFP*)- and *TNF* (*BFP*)-encoding retroviral particles with the use of RetroNectin reagent (Takara Bio) and spinfection. At day 2 post transduction, MS5 cells were sorted based on co-expression of GFP and BFP. Expression of DLL4 (clone MHD4-46) and tmTNF (clone Mab11) were validated by flow cytometry.

OP9 and MS5 co-cultures

To study the regulation of *IRF8* expression by Notch signalling, lin^-CD34^+ HSPCs were sorted and co-cultured with OP9 stromal cells that express GFP only (control) or different human Notch ligands. The co-culture medium used was described previously and supplemented with SCF, FLT3-L and IL-7 (all 5 ng/mL) in order to promote T cell development (Dolens et al., 2016). At day 3, differentiating $CD45^+$ HSPCs were sorted for analysis by quantitative reverse transcription PCR (RT-qPCR).

To determine the developmental potential of CD123-expressing thymic progenitors, thymic CD34-enriched cells were stained with antibodies against the lineage markers (lin: as defined above), CD4 (clone RPA-T4), CD34 (clone 581), CD123 (clone AC145) and CD1a (clone HI149), and sorted into 4 subsets ($lin^-CD4^-CD34^+$: $CD123^{hi}CD1a^-$, $CD123^{lo}CD1a^-$, $CD123^-CD1a^-$ and $CD123^-CD1a^+$). All subsets were co-cultured with OP9 stromal cells that express

GFP only or DLL4. OP9 co-cultures were supplemented with 20 ng/mL SCF, 100 ng/mL FLT3-L and 20 ng/mL granulocyte-macrophage colony-stimulating factor (GM-CSF) to induce dendritic cell development. OP9-DLL4 co-cultures were supplemented with T-stimulating cytokine as described above.

To investigate the impact of constitutive expression of *IRF8* on T cell development, cord blood-derived CD34-enriched cells were transduced with LZRS-IRES-EGFP (control) or LZRS-IRF8-IRES-EGFP. $CD123^{-}lin^{-}CD34^{+}GFP^{+}$ HSPCs were sorted and co-cultured with OP9-DLL4 stromal cells in T-stimulating culture conditions as described above.

Similarly, to examine the dose-dependent impact of IRF8 on T cell development, cord blood HSPCs transduced with the control or LZRS-IRF8-ERT2-P2A-EGFP were sorted for $CD123^{-}lin^{-}CD34^{+}GFP^{+}$ and co-cultured with OP9-DLL4 stromal cells. Cells were treated with 4-hydroxytamoxifen (4-OHT: Sigma-Aldrich, cat. SML1666) at day 0 and day 3 post co-culture. For 0 nM condition, cells were treated with the compound solvent at a final concentration equivalent to the highest tested dose of 4-OHT (300 nM). Differentiating HSPCs were analysed or sorted for downstream experiments at the indicated time points.

For co-cultures with OP9-DLL4-7FS stromal cells that express human SCF, FLT3-L and IL-7, the MEMα medium containing 5 % fetal calf serum, 100 units/mL penicillin, 100 µg/mL streptomycin and 2 mM L-glutamine was not supplemented with additional cytokines. Half of the existing medium was replaced with fresh medium every 3-4 days till analysis.

To determine the impact of TNFR2 expression on the development of myeloid cells, the sorted HSPCs were co-cultured with MS5 stromal cells as described previously with the supplementation of 20 ng/mL FLT3-L, 20 ng/mL SCF, 20 ng/mL TPO, 10 ng/mL GM-CSF and 10 ng/mL granulocyte colony-stimulating factor (G-CSF) (De Decker et al., 2021).

RNA extraction and RT-qPCR

Total RNA from sorted cells was extracted using miRNeasy Micro Kit (Qiagen, cat. 217084), with removal of contaminating DNA by DNase digestion (Qiagen, cat. 79254), and converted into cDNA using iScript cDNA Synthesis Kit (Bio-Rad, cat. 1708890). Whenever it was necessary, target-specific pre-amplification of cDNA was performed using SsoAdvanced SYBR Green Supermix (Bio-Rad, cat. 1725271). Real-time PCR reactions were performed using LightCycler 480 SYBR Green I Master Mix (Roche, cat. 04707516001) and were run on a LightCycler 480 system (Roche). Specific amplification of target was confirmed by melting curve analysis. Gene expression was calculated using the $2^{-\Delta\Delta Ct}$ method. Primer sequences are provided in the Supplementary Information.

TCRD genomic rearrangement

DNA was extracted from the sorted cells and HL-60 cell line using GenElute Mammalian Genomic DNA Purification Kit (Sigma-Aldrich, cat. G1N350). DNA from the $CD123^{hi}(IRF8^{hi})CD1a^{-}$ sorted cells was extracted using homemade tail lysis buffer with proteinase K digestion. Purified DNA was concentrated by ethanol precipitation. Dδ2-Dδ3 recombination was detected using the previously described primer (Dδ2: 5'-CAAGGAAAGGGAAAAAGGAAGAA-3'; Dδ3: 5'-TTGCCCCTGCAGTTTTTGTAC-3') and probe (Dδ3: 5'-/FAM/ATACGCACA/ZEN/GTGCTACAAAACCTACAGAGACCT/IBFQ/-3' (IDT) sequences (Dik et al., 2005). Dδ2-Dδ3 recombination was normalized against the *Albumin* gene (forward: 5'-TGAACAGGCGACCATGCTT-3'; reverse: 5'-CTCTCCTTCTCAGAAAGTGTGCATAT-3'; probe: 5'-/FAM/TGCTGAAAC/ZEN/ATTCACCTTCCATGCAGA/IBFQ/-3') (IDT) (Dik et al., 2005)

and quantified using the $2^{-\Delta\Delta Ct}$ method. qPCR was performed using the PrimeTime Gene Expression Master Mix (IDT) with 500 nM of each primer and 200 nM of probe. qPCR was run on a LightCycler 480 system (Roche).

Analysis of bulk RNA-seq data

Total RNA from the sorted co-cultured cells was extracted as described above. mRNA libraries were prepared using QuantSeq 3' mRNA-Seq Library Prep Kit FWD (Lexogen) and sequenced as single-end 75 bp reads on the NextSeq 500 System (Illumina). The average total reads per sample is 8.8 ± 1.3 million. All the reads were trimmed using Cutadapt to remove the adaptor sequences, and mapped against Homo sapiens GRCh38 reference genome using STAR (Dobin et al., 2013; Martin, 2011). A table of read counts for quantifiable genes was generated using RSEM (Li and Dewey, 2011). Differential gene expression analysis between groups of samples was performed using edgeR with batch effect correction due to inter-donor variability (Robinson et al., 2010). Volcano plots were generated in R. Clustered heatmaps were constructed in R, where normalized counts of significantly differentially expressed genes were rescaled as standard deviations from the mean (Z-scores), between -2 and 2, and clustered based on Pearson correlation. 17 genes that were statistically significantly downregulated in the presence of low level of inducible IRF8 activity constituted the interferon-related gene set.

Analysis of bulk ATAC-seq data

Genomic DNA from the sorted co-cultured cells was tagmented by Tn5 transposase and DNA libraries were made as described previously (Roels et al., 2020). Paired-end sequencing was done on the Illumina NextSeq500 sequencer with a 75 bp read output. The quality of the sequencing was verified with FastQC. Reads were trimmed using NGMerge (Gaspar, 2018).

Alignment was done using Bowtie2 (v2.2.6) with parameter --very-sensitive, using the human hg38 reference genome (Langmead and Salzberg, 2012; Langmead et al., 2019). Duplicate reads were removed using SAMTools. Peak calling was performed with MACS2 (v2.1.2) and the option --no-model. Significant peaks at an adjusted *p*-value cut-off of 0.05 were combined into one matrix across all samples, with merging of peaks that show at least 50 percent overlap. The function SummarizeOverlaps of the GenomicAlignments package in R was used for read counting using this matrix and the BAM files (Lawrence et al., 2013). DESeq2 was used to detect significantly differential opened chromatin sites between samples, using a design containing replicate and condition (Love et al., 2014). An adjusted *p*-value of 0.05 was used to retain significant hits. Homer findMotifsGenome was used for motif enrichment analysis on significantly different opened chromatin regions (Heinz et al., 2010).

Embryonic mesodermal organoid (EMO) cultures

To induce hematopoietic specification, embryonic mesodermal progenitors (EMPs) derived from iPSCs were aggregated with MS5-DLL4 stromal cells to form EMOs. EMPs were generated and isolated as described previously (Montel-Hagen et al., 2019). EMOs were assembled and cultured as described previously (Montel-Hagen et al., 2019). After two weeks of culture, EMOs were cultured further in T-stimulating conditions (Montel-Hagen et al., 2019) or harvested by forceful pipetting for downstream experiments (flow cytometry, limiting dilution or ATO-spiking analyses).

Limiting dilution analysis

10 (48 wells), 25 (48 wells), 50 (24 wells) and 100 (24 wells) of $TNFR2^{+}CD123^{+}$ hematopoietic progenitors derived from *IRF8*$^{+/+}$ EMOs were sorted by single cell precision mode for direct

co-culture with OP9-DLL4-7FS stromal cells. At day 14, the developmental potential of TNFR2^{+}CD123^{+} hematopoietic progenitors was calculated (Hu and Smyth, 2009) by analysing each well for the development of T, dendritic cell or both lineages. Only wells in which more than 10 CD45^{+} cells were detected by flow cytometry were scored. The plating efficiency was 33.3 % for 10 cells seeded, 81.3 % for 25 cells seeded, 79.2 % for 50 cells seeded and 100 % for 100 cells seeded.

Detection of soluble TNF (sTNF)

At day 14, medium from EMO cultures were centrifuged at 1,500 x g at 4 °C for 10 minutes. Aliquots of supernatant (conditioned medium) were stored in protein Lobind tubes (Eppendort, cat. EP0030108116) at -80 °C for single use (Lehmann et al., 2017). Presence of sTNF in the conditioned medium was detected by LEGENDplex assay with the Human Adipokine Panel (BioLegend). All samples and serially diluted controls were run in duplicates. Data was analysed by LEGENDplex software version 8.

Culture of EMOs using conditioned medium

Conditioned medium from void, WT and KO EMOs, at day 9, 11 and 14 post culture, was collected as described above and used to culture *IRF8*$^{-/-}$ EMOs at day 7, 9 and 11, respectively. *IRF8*$^{+/+}$ and *IRF8*$^{-/-}$ EMOs cultured with fresh medium served as positive and negative controls, respectively. Both fresh and conditioned media were supplemented with 50 ng/mL SCF, 5 ng/mL FLT3-L, 5 ng/mL TPO and 10 µM TGF-βRI inhibitor SB-431542SB as described previously (Montel-Hagen et al., 2019). At day 14, cells were harvested for flow cytometric analyses.

Artificial thymic organoid (ATO) cultures

ATOs were assembled and cultured with the supplementation of 5 ng/mL FLT3-L and IL-7 as described previously, but with the exception that DLL4 instead of DLL1 was used to support T cell development (Seet et al., 2017). As indicated in the individual experiments, ATOs were assembled using MS5-DLL4 or MS5-DLL4/tmTNF stromal cells or in combination at different ratios. Per ATO, up to 7,500 HSPCs were aggregated with a total amount of 150,000 stromal cells. Whenever indicated, ATOs were cultured and refreshed with medium without the supplementation of 5 ng/mL IL-7, with the supplementation of sTNF (0.25, 5 or 100 ng/mL) (Miltenyi Biotec, cat. 130-094-015) or with the supplementation of 10 ng/mL EHD2-scTNF$_{R2}$ (Dong et al., 2016). Whenever indicated, ATOs were spiked with CD123-expressing hematopoietic cells (1,450 iPSC-derived CD123$^+$ cells and 7,500 HSPCs in an ATO). For secondary ATO cultures, CD45$^+$CD7$^+$ differentiating cord blood HSPCs were sorted into 96-well conical bottom plate using single cell mode (3,500 cells per well). Subsequently, 150,000 stromal cells were added per well to assemble an ATO. At indicated time points, cells were harvested from ATO by forceful pipetting for flow cytometry analyses.

Analysis of scRNA-seq data

Cord blood HSPCs were differentiating in ATOs in the absence (control) or presence of TNF stimulus (sTNF at 0.25 ng/mL or tmTNF-expressing stromal cells at 1 %). At day 10 post culture, CD45$^+$ cells were sorted from all conditions for scRNA-seq where libraries were prepared and sequenced according to the Chromium Single Cell Gene Expression workflow. Using CellRanger 6.0.1, the sequencing data was mapped against the GRCh38 genome. The filtered feature-barcode matrices were loaded into R. Low quality cells were identified as

having less than 200 genes, more than 6000 genes (doublets) or more than 5 % mitochondrial reads. Low quality genes were identified as being expressed in less than 3 cells. Both low quality cells and genes were removed. Equal number of cells were sub-sampled from all 3 ATO conditions and integrated (total: 38,439 cells) prior clustering using Seurat (Butler et al., 2018). The UMAP method was used to visualize the cell clusters (Mclnnes et al., 2018). The two smallest clusters (26: 0.22% and 27: 0.17%) were removed from the original identified 28 clusters. Cell cycle status of the remaining 26 clusters (38,290 cells: 0 to 25) were determined using the CellCycleScoring function from the Seurat library (Hao et al., 2021). These 26 clusters were manually annotated based on cell type-specific markers genes that are differentially expressed as determined by using FindAllMarkers from Seurat. Dot plot was used to visualize the expression of cell type-specific marker genes. UCell (Andreatta and Carmona, 2021) was used to score the interferon-related gene signature derived from the bulk RNA-seq data analysis. The average expression values for the interferon-related genes were calculated using the AverageExpression function from the Seurat library (Hao et al., 2021) and visualized in a clustered heatmap that was constructed using the pheatmap library in R.

Flow cytometric analysis

Fully stained samples were measured on a BD LSR II flow cytometer or a BD FACSymphony A3 Cell Analyzer. Both are equipped with violet (405 nm), blue (488 nm), yellow-green (561 nm) and red (640 nm) lasers. Cells were sorted on a BD FACSAria II or BD FACSAria Fusion flow cytometers. UltraComp eBeads (Thermo Fisher Scientific, cat. 01-2222-41) were used to prepare single-color compensation controls for all antibodies used, whereas living and dead Jurkat cells were used as a control to compensate for the spillover of propidium iodide or fixable viability dye eFluor506. Flow cytometric data were visualized and analyzed using BD FlowJo

v10. Doublets, aggregates and dead cells were excluded from analyses. Gating strategies for cell sorting are provided in the Supplementary Information.

Statistics

GraphPad Prism 9 was used for statistical analyses and graphing. Data with replicates of 3 or more were presented as mean±s.d. All measurements were taken from distinct donors except experiments that involved iPSCs. The Gaussian distribution of data residuals was examined visually by a Quantile-Quantile normality plot and with Shapiro-Wilk statistical test. Depending on the data normality, parametric or non-parametric statistical tests were applied and indicated in the figure legends.

Data availability

The datasets generated and/or analysed in this study are available in the Gene Expression Omnibus with the following accession numbers: *ex vivo* human $CD34^+$ thymocytes for scRNA-seq (GSE144870), 4-OHT-treated OP9-DLL4 co-cultures for ATAC-seq (GSE179534) and RNA-seq (GSE179381), and TNF-activated ATO cultures for scRNA-seq (GSE211400).

FIGURE LEGENDS

Figure 1. TSP2- and HPC-annotated CD34$^+$ human thymocytes express low levels of IRF8 and are bi-phenotypic and potent for T- and DC-lineages.

(A) Scheme summarizes the developmental trajectories of the previously annotated CD34$^+$ postnatal thymocytes for T- and DC-lineages (Lavaert et al., 2020).

(B) mRNA expression of *IRF8* and *IL3RA* for the annotated populations of thymocytes shown in (A). The number of cells for each population is indicated above the violin plot.

(C) Flow cytometric gating of *ex vivo* lin$^-$CD4$^-$CD34$^+$ thymocytes (n = 8) based on their expression level of IRF8 and CD1a.

(D-E) Frequencies (D) of the cellular subsets identified in (C) and their protein expression profiles (F) for immature (top), T (middle) and DC (bottom) markers.

(F) Heatmap illustrates the relative mRNA expression of the additional markers that are shown in (E) for the annotated CD34$^+$ thymocyte populations that correspond to the cellular subsets identified in (C).

(G) Protein expression profile of lin$^-$CD4$^-$CD34$^+$ thymocytes for PU.1 and CD123 (n = 2), and is coloured to display median fluorescence intensity of IRF8 (left) and GATA3 (right). The arrow head indicates cells at the bifurcation of T- and DC-lineages that express low levels of IRF8 (Figure S1C).

(H-I) The sorted subsets (n = 3), as in (Figure S1F: top), were co-cultured with OP9-DLL4 stromal cells. Flow cytometry analysis to identify CD7$^+$CD5^{hi} T cell precursors (H) and their normalized absolute counts (I).

(J-K) The sorted subsets (n = 3), as in (Figure S1F: top), were co-cultured with OP9 stromal cells that express GFP only. Flow cytometry analysis to identify HLA-DR$^+$CD1c$^+$ cDCs and HLA-DR$^+$CD123$^+$ pDCs (J), and their absolute counts (K).

(L) Probe-based qPCR analysis to determine the relative frequency of *TCRD* rearrangement in the sorted immature (n = 2 as in Figure S1F: top, except n = 3 for CD123^{hi}CD1a^{-} subset) and mature (n = 3 for cDCs, pDCs, B cells and αβ T cells) *ex vivo* hematopoietic cells. HL-60, a promyelocytic leukaemia cell line, served as a negative control.

Representative of two (E, G), eight (C) and three (H, J) independent experiments; Mean±s.d. of eight (D), three (I, K) and one (L: CD123^{hi}CD1a^{-} subset and mature cells) independent experiments; Mean of one experiment (L: immature cells except CD123^{hi}CD1a^{-} subset); Two-way ANOVA with Šídák's multiple comparisons test (K); DC, dendritic cell; TSP, thymus seeding progenitor; ETP, early T cell precursor; HPC, hematopoietic progenitor cell; GMP, granulocyte-macrophage progenitor; pDC, plasmacytoid dendritic cell; cDC, conventional dendritic cell; lin, lineage; cyCD3, cytoplasmic CD3; *n*, donor.

Figure 2. IRF8 expression is induced during human T-lineage specification but is silenced in the subsequent commitment stage.

(A) Relative mRNA expression of *IRF8* for cord blood HSPCs (n = 2), co-cultured for 3 days on OP9 stromal cells that express GFP only (control) or different human Notch ligands.

(B) Flow cytometric analysis of IRF8 expression in cord blood HSPCs (n = 5) that were transduced with empty vector (control) or ICN1.

(C) Frequency of IRF8^{+} cells identified in (B).

(D) Expression of CD10 and CD127 for the IRF8^{-} and IRF8^{+} fractions identified in (B).

(E) Flow cytometric staining for CD7^{+}CD5^{lo} and CD7^{+}CD5^{hi} T cell precursors generated from control and IRF8 transduced cord blood-derived HSPCs in OP9-DLL4 co-culture (n = 3) at day 14.

(F-G) Frequency (F) of T cell precursors identified in (E) and their expression for CD1a (G).

(H) Flow cytometric staining of IRF8 and GATA3 expression in *ex vivo* human thymic progenitors (n = 8).

(I-K) IRF8 expression, at mRNA (I: n = 3) and protein level (J-K: n = 4), in HSPCs that overexpressed empty vector (control) and GATA3 at day 2 post transduction.

(L) mRNA expression of *IRF8* and *GATA3* in empty vector (control) and *GATA3* shRNA-expressing HSPCs (n = 3) at day 2 post transduction.

Representative of two (B, D, E, G, J) and eight (H) independent experiments; Mean of two independent experiments (A); Mean±s.d. of two independent experiments (C, F, I, K, L); Two-tailed paired t test (C, I, K, L); Two-way ANOVA with Šídák's multiple comparisons test (F); lin, lineage; GFP, green fluorescent protein; ICN1, intracellular NOTCH1; HSPCs, hematopoietic stem and progenitor cells; shRNA, short hairpin RNA; n, donor.

Figure 3. Low dose of active IRF8 promotes generation of tmTNF-expressing CD7$^+$CD123$^+$ progenitors and T cell precursors.

(A) Scheme illustrates the downstream independent analyses of empty vector (control) or IRF8-ERT2-transduced HSPCs that were co-cultured with OP9-DLL4 stromal cells.

(B-D) Flow cytometric analyses of the transduced cells (n = 4), treated without or with increasing doses of 4-OHT. T cell precursors were identified as CD7$^+$CD5$^+$ whereas the CD7$^+$CD5$^-$ cellular fraction was examined further to identify cells that co-express CD34 and CD123 (B). Absolute counts of CD7$^+$CD5$^+$ T cell precursors (C) and CD7$^+$CD123$^+$ progenitors (D) identified in (B).

(E) Bulk RNA-seq (n = 3) analysis to determine IRF8-mediated changes in the transcriptional landscape of CD7$^+$ cells. Genes that were significantly downregulated in the presence of low dose of inducible IRF8 activity constituted the interferon (IFN)-related gene signature.

(F) IFN-related gene signature was scored in the previously annotated populations of *ex vivo* $CD34^+$ thymocytes.

(G) ATAC-seq (n = 3) analysis to identify IRF8-mediated changes in the chromatin accessibility landscape of $CD34^+CD7^-$ and $CD7^+$ cells.

(H) Genome browser view of ATAC-seq footprint around the *CEBPE* and *TNF* gene locus.

(I-J) Flow cytometric analysis (n = 3) to examine the expression of tmTNF and TNF receptor 2 (TNFR2) during early T cell development (I) and their expression patterns were quantified proportionally (J).

Mean±s.d. of three (C, D) and one (J) independent experiments; Representative of three (B) and one (I) independent experiments; One-way ANOVA with Dunnett's multiple comparisons test (C, D); Two-way ANOVA with Šídák's multiple comparisons test (J); 4-OHT, 4-hydroxytamoxifen; GFP, green fluorescent protein; IFN, interferon; tmTNF, transmembrane TNF; n, donor.

Figure 4. IRF8-dependent DC-biased $CD123^+CD127^+$ progenitors express tmTNF and augments generation of T cell precursors via cellular crosstalk.

(A) Scheme of EMO assembly for hematopoietic and T-induction of iPSC-derived EMPs.

(B) Flow cytometric analysis to identify $CD7^+CD5^+$ T cell precursors and the more mature $CD4^+CD8b^+$ subset.

(C) Quantification of the cells identified in (B) (n = 4; 8 EMOs per genotype).

(D) Scheme of the downstream independent analyses performed on the iPSC-derived hematopoietic progenitors.

(E) Flow cytometric analysis to determine the impact of IRF8 loss on the generation of $TNFR2^+CD123^+CD127^+$ hematopoietic progenitors.

(F) Quantification of the progenitors identified in (E) (n = 8; 16 EMOs per genotype).

(G) Characterization of IRF8 tmTNF expression in $CD123^+CD127^+$ vs $CD123^-CD127^-$ cells within $CD45^+CD34^+TNFR2^+$ gated precursors in the *IRF8*$^{+/+}$ EMOs (n = 4; 8 EMOs in total).

(H-I) Comparison of tmTNF expression in $CD45^+CD34^+TNFR2^+$ $CD123^+CD127^+$ gated cells in *IRF8*$^{+/+}$ versus *IRF8*$^{-/-}$ EMOs (H) and quantification of the expression of tmTNF (n = 4; 8 EMOs per genotype).

(J-K) 10, 25, 50 and 100 of iPSC-derived $TNFR2^+CD123^+$ hematopoietic progenitors were sorted for co-culture with OP9-DLL4-7FS stromal cells. At day 14, flow cytometric analysis were performed to identify cells of T- and DC-lineages (J), and lineage potential of the sorted cells was calculated by the ELDA software (Hu and Smyth, 2009) (K).

(L) Scheme illustrates the assembly of ATOs without (control) or with the spiking of iPSC-derived $TNFR2^+CD123^+$ hematopoietic progenitors.

(M) At day 10 post culture, flow cytometric analyses to identify $CD7^+CD5^+$ T cell precursors generated from cord blood-derived $lin^-CD34^+CD38^-$ HSPCs (n = 3; HLA-$A2^-$) or iPSC-derived $TNFR2^+CD123^+$ hematopoietic progenitors (HLA-$A2^+$).

(N-O) Relative qQuantification of the frequency and number of T cell precursors generated from HSPCs in the spiked-ATOs compared to the control (N) and flow cytometric analysis of their CD1a expression (O).

Mean±s.d. of one (C, N), three (F) and two (I) independent experiments; Representative of one (B, M, O), three (E), two (G) and five (H) independent experiments; Two-tailed paired t test (F, I); One sample two-tailed t test (N); iPSC, induced pluripotent stem cell; EMP, embryonic mesodermal progenitor; EMO, embryonic mesodermal organoid; tmTNF, transmembrane TNF; DC, dendritic cell, CI, confidence interval; lin, lineage; ATO, artificial thymic organoid; FC, fold change; n, pool of 2 EMOs except (M).

Figure 5. Expression of TNFR2 precedes induction of CD7 during early human T cell development.

(A) Flow cytometric analysis to identify 5 cellular subsets (labelled 1-5) of *ex vivo* $lin^-CD4^-CD34^+$ thymocytes.

(B) The developmental relationship (left) between all 5 annotated cellular subsets identified in (A) and their expression of TNFR1, TNFR2, tmTNF and CD127 (right; $n = 4$).

(C) ATOs were assembled using HSPCs derived from human fetal liver ($CD34^{hi}CD45^+$; $n = 2$), cord blood ($lin^-CD34^+CD38^-$; $n = 2$) or adult buffy coats (lin^-CD34^+; $n = 4$), and harvested for flow cytometry analyses at day 2, 4, 7 and 10 post culture. For each ontogenetic stage, expression of TNFR2 and CD7 is shown in representative contour plots.

(D) Quantification of the proportional changes in the 4 cellular subsets shown in (C) throughout the culture period.

(E) Expression of CD5 on the 4 cellular subsets of buffy coat-ATOs at day 10 post culture is shown in representative offsetting histograms.

(F-G) At day 10 post culture, cord blood-ATO ($lin^-CD34^+CD38^-$; $n = 3$) supplemented with and without IL-7 were immunophenotyped for the expression of TNFR2 and CD7 (F), and proportional changes in the 4 cellular subsets were quantified (G).

(H) The subset comprised of $TNFR2^+CD7^+$ cells were examined further for the expression of CD5 and CD123.

(I) $TNFR2^-$ and $TNFR2^+$ fractions were sorted from cord blood HSPCs (lin^-CD34^+; $n = 3$) and cultured in the ATO system in the presence of tmTNF stimulus for 10 days or co-cultured with MS5 stromal cells for 14 days.

(J-K) Flow cytometric analysis of TNF-activated ATO cultures to identify $CD7^+CD5^+$ T cell precursors (J) and their absolute counts (K).

(L-M) Flow cytometric analysis of MS5 co-cultures to identify $CD15^+CD14^-$ granulocytes, $CD15^-CD14^+$ monocytes and $CD34^+$ immature progenitors (L), and their absolute counts (M). ATOs from each ontogenetic stage (mean for fetal liver and cord blood; mean±s.d. for buffy coat) were assembled and analysed independently (D~~C~~); Mean±s.d. (B, G, K, M) and representative (A, C, E-F, H-J, L) of one experiment; One-way ANOVA with linear trend test for each subsets (D); Two-way ANOVA with Šídák's multiple comparisons test (G, M); Two-tailed paired t test (K); ATO, artificial thymic organoid; IL-7, interleukin 7; lin, lineage; *n*, donor.

Figure 6. Selective targeting of TNFR2 enhances *in vitro* generation of T cell precursors.

(A) Scheme of ATO assembly using MS5-DLL4 (control) or MS5-DLL4/tmTNF, or a combination of both at different ratios. The ATOs were analysed by flow cytometry after 10 days of culture (cord blood $lin^-CD34^+CD38^-$; $n = 4$).

(B) Absolute counts of $CD45^+$ cells harvested from an ATO that was aggregated with a normalized amount of 7,500 HSPCs.

(C-D) Flow cytometric identification of $CD7^+CD5^+$ T cell precursors (C) that were generated from HSPCs, of which some remained undifferentiated and expressed CD34 (D).

(E) Quantification of the impact of tmTNF signal intensity on the cell counts of T cell precursors and undifferentiated $CD34^+$ HSPCs compared to the control.

(F-G) Flow cytometric analysis of the HLA-DR expression profiles of CD1a-expressing T cell precursors (F) and quantification of the cellular fractions that were positive (G).

(H) Flow cytometric analysis of ATO cultures (adult buffy coat lin^-CD34^+; $n = 7$) at day 10 to determine the impact of EHD2-$scTNF_{R2}$ (TNFR2 selective agonist) on the generation of $CD7^+CD5^+$ T cell precursors.

(I) Relative qQuantification of the frequency and cell counts of T cell precursors generated in TNFR2-activated conditions compared to the control.

Mean±s.d. (B, E, G, I) and representative (C, D, F, H) of two independent experiments; One-way ANOVA with linear trend test (E); Friedman test with Dunnett's post-hoc analysis (G); One sample two-tailed t test (I); tmTNF, transmembrane TNF; ATO, artificial thymic organoid; FC, fold change; lin, lineage; *n*, donor.

Figure 7. TNF-activated lymphoid progenitors downregulates expression of interferon-related genes and are competent in T-lineage development.

(A) Scheme illustrates single-cell RNA sequencing of $CD45^+$ differentiating cells (cord blood lin^-CD34^+; $n = 4$) derived from ATOs without (control) and with TNF stimulus (sTNF at 0.25 ng/mL or tmTNF-expressing stromal cells at 1 %).

(B) UMAP visualization of the 26 cellular clusters (labelled 0 to 25) comprising $CD45^+$ differentiating cells derived from all conditions.

(C) All clusters identified in (B) were annotated based on their expression profiles of cell type-specific marker genes as shown in the dot plot.

(D) The frequency of all the annotated populations of hematopoietic cells (top) and the relative distribution of cells derived from different ATO conditions in each of these populations (bottom).

(E) UMAP visualization of the enrichment of IFN-related gene signature across all the cellular clusters.

(F) Clustered heatmap shows the average expression of IFN-related genes by lymphoid progenitors (cluster 4 and 15) derived from different ATO conditions.

(G) Scheme illustrates the experimental design where $CD7^+$ T-specified progenitors derived from ATOs (cord blood lin^-CD34^+; $n = 5$) without (control) or with TNF stimulus (sTNF at 0.25 ng/mL or tmTNF-expressing stromal cells at 1%) were examined for their maturation potential towards later stages of T-lineage development.

(H-I) Flow cytometric analysis at day 13 post secondary ATO culture to identify $CD4^+CD8b^+$ thymocytes (H). Relative qQuantification of the frequency and cell counts of the identified cells derived from TNF-activated progenitors compared to the control (I).

(J-L) Flow cytometric analysis at day 25 post secondary ATO culture to identify $CD3^+TCR\alpha\beta^+$ and $CD3^+TCR\gamma\delta^+$ T cells (J). Relative qQuantification of the frequency and cell counts of the identified cells derived from TNF-activated progenitors compared to the control (K-L).

Mean±s.d. (I, K, L) and representative (H, J) of two independent experiments; One sample two-tailed t test (K-L); sTNF, soluble TNF; tmTNF, transmembrane TNF; ATO, artificial thymic organoid; lin, lineage; *n*, donor.

REFERENCES

Aggarwal, S., Gollapudi, S., and Gupta, S. (1999). Increased TNF-alpha-induced apoptosis in lymphocytes from aged humans: changes in TNF-alpha receptor expression and activation of caspases. J Immunol *162*, 2154-2161.

Andreatta, M., and Carmona, S.J. (2021). UCell: Robust and scalable single-cell gene signature scoring. Comput Struct Biotechnol J *19*, 3796-3798.

Azzawi, M., and Hasleton, P. (1999). Tumour necrosis factor alpha and the cardiovascular system: its role in cardiac allograft rejection and heart disease. Cardiovasc Res *43*, 850-859.

Balan, S., Arnold-Schrauf, C., Abbas, A., Couespel, N., Savoret, J., Imperatore, F., Villani, A.C., Vu Manh, T.P., Bhardwaj, N., and Dalod, M. (2018). Large-Scale Human Dendritic Cell Differentiation Revealing Notch-Dependent Lineage Bifurcation and Heterogeneity. Cell Rep *24*, 1902-1915 e1906.

Benz, C., Martins, V.C., Radtke, F., and Bleul, C.C. (2008). The stream of precursors that colonizes the thymus proceeds selectively through the early T lineage precursor stage of T cell development. J Exp Med *205*, 1187-1199.

Black, R.A., Rauch, C.T., Kozlosky, C.J., Peschon, J.J., Slack, J.L., Wolfson, M.F., Castner, B.J., Stocking, K.L., Reddy, P., Srinivasan, S.*, et al.* (1997). A metalloproteinase disintegrin that releases tumour-necrosis factor-alpha from cells. Nature *385*, 729-733.

Blom, B., and Spits, H. (2006). Development of human lymphoid cells. Annu Rev Immunol *24*, 287-320.

Butler, A., Hoffman, P., Smibert, P., Papalexi, E., and Satija, R. (2018). Integrating single-cell transcriptomic data across different conditions, technologies, and species. Nat Biotechnol *36*, 411-420.

Cante-Barrett, K., Mendes, R.D., Li, Y., Vroegindeweij, E., Pike-Overzet, K., Wabeke, T., Langerak, A.W., Pieters, R., Staal, F.J., and Meijerink, J.P. (2017). Loss of CD44(dim) Expression from Early Progenitor Cells Marks T-Cell Lineage Commitment in the Human Thymus. Front Immunol *8*, 32.

Chen, E.L.Y., Brauer, P.M., Martinez, E.C., Huang, X., Yu, N., Anderson, M.K., Li, Y., and Zuniga-Pflucker, J.C. (2021). Cutting Edge: TCR-beta Selection Is Required at the CD4(+)CD8(+) Stage of Human T Cell Development. J Immunol *206*, 2271-2276.

Cieslak, A., Le Noir, S., Trinquand, A., Lhermitte, L., Franchini, D.M., Villarese, P., Gon, S., Bond, J., Simonin, M., Vanhille, L.*, et al.* (2014). RUNX1-dependent RAG1 deposition instigates human TCR-delta locus rearrangement. J Exp Med *211*, 1821-1832.

Cytlak, U., Resteu, A., Pagan, S., Green, K., Milne, P., Maisuria, S., McDonald, D., Hulme, G., Filby, A., Carpenter, B.*, et al.* (2020). Differential IRF8 Transcription Factor Requirement Defines Two Pathways of Dendritic Cell Development in Humans. Immunity *53*, 353-370 e358.

De Decker, M., Lavaert, M., Roels, J., Tilleman, L., Vandekerckhove, B., Leclercq, G., Van Nieuwerburgh, F., Van Vlierberghe, P., and Taghon, T. (2021). HES1 and HES4 have non-redundant roles downstream of Notch during early human T-cell development. Haematologica *106*, 130-141.

De Smedt, M., Leclercq, G., Vandekerckhove, B., Kerre, T., Taghon, T., and Plum, J. (2011). T-lymphoid differentiation potential measured in vitro is higher in CD34+CD38-/lo hematopoietic stem cells from umbilical cord blood than from bone marrow and is an intrinsic property of the cells. Haematologica *96*, 646-654.

De Smedt, M., Reynvoet, K., Kerre, T., Taghon, T., Verhasselt, B., Vandekerckhove, B., Leclercq, G., and Plum, J. (2002). Active form of Notch imposes T cell fate in human progenitor cells. J Immunol *169*, 3021-3029.

Dik, W.A., Pike-Overzet, K., Weerkamp, F., de Ridder, D., de Haas, E.F., Baert, M.R., van der Spek, P., Koster, E.E., Reinders, M.J., van Dongen, J.J.*, et al.* (2005). New insights on human T cell development by quantitative T cell receptor gene rearrangement studies and gene expression profiling. J Exp Med *201*, 1715-1723.

Diwan, A., Dibbs, Z., Nemoto, S., DeFreitas, G., Carabello, B.A., Sivasubramanian, N., Wilson, E.M., Spinale, F.G., and Mann, D.L. (2004). Targeted overexpression of noncleavable and secreted forms of tumor necrosis factor provokes disparate cardiac phenotypes. Circulation *109*, 262-268.

1172 Dobin, A., Davis, C.A., Schlesinger, F., Drenkow, J., Zaleski, C., Jha, S., Batut, P., Chaisson,
1173 M., and Gingeras, T.R. (2013). STAR: ultrafast universal RNA-seq aligner. Bioinformatics *29*,
1174 15-21.
1175
1176 Dolens, A.C., Durinck, K., Lavaert, M., Van der Meulen, J., Velghe, I., De Medts, J., Weening,
1177 K., Roels, J., De Mulder, K., Volders, P.J.*, et al.* (2020). Distinct Notch1 and BCL11B
1178 requirements mediate human gammadelta/alphabeta T cell development. EMBO Rep *21*,
1179 e49006.
1180
1181 Dolens, A.C., Van de Walle, I., and Taghon, T. (2016). Approaches to Study Human T Cell
1182 Development. Methods Mol Biol *1323*, 239-251.
1183
1184 Dong, Y., Fischer, R., Naude, P.J., Maier, O., Nyakas, C., Duffey, M., Van der Zee, E.A.,
1185 Dekens, D., Douwenga, W., Herrmann, A.*, et al.* (2016). Essential protective role of tumor
1186 necrosis factor receptor 2 in neurodegeneration. Proc Natl Acad Sci U S A *113*, 12304-12309.
1187
1188 Dos Santos Schiavinato, J.L., Oliveira, L.H., Araujo, A.G., Orellana, M.D., de Palma, P.V.,
1189 Covas, D.T., Zago, M.A., and Panepucci, R.A. (2016). TNF-alpha and Notch signaling
1190 regulates the expression of HOXB4 and GATA3 during early T lymphopoiesis. In Vitro Cell
1191 Dev Biol Anim *52*, 920-934.
1192
1193 Dybedal, I., Bryder, D., Fossum, A., Rusten, L.S., and Jacobsen, S.E. (2001). Tumor necrosis
1194 factor (TNF)-mediated activation of the p55 TNF receptor negatively regulates maintenance of
1195 cycling reconstituting human hematopoietic stem cells. Blood *98*, 1782-1791.

Edgar, J.M., Michaels, Y.S., and Zandstra, P.W. (2022). Multi-objective optimization reveals time- and dose-dependent inflammatory cytokine-mediated regulation of human stem cell derived T-cell development. NPJ Regen Med *7*, 11.

Feil, R., Wagner, J., Metzger, D., and Chambon, P. (1997). Regulation of Cre recombinase activity by mutated estrogen receptor ligand-binding domains. Biochem Biophys Res Commun *237*, 752-757.

Fischer, R., Kontermann, R.E., and Pfizenmaier, K. (2020). Selective Targeting of TNF Receptors as a Novel Therapeutic Approach. Front Cell Dev Biol *8*, 401.

Gaspar, J.M. (2018). NGmerge: merging paired-end reads via novel empirically-derived models of sequencing errors. BMC Bioinformatics *19*, 536.

Grell, M., Douni, E., Wajant, H., Lohden, M., Clauss, M., Maxeiner, B., Georgopoulos, S., Lesslauer, W., Kollias, G., Pfizenmaier, K.*, et al.* (1995). The transmembrane form of tumor necrosis factor is the prime activating ligand of the 80 kDa tumor necrosis factor receptor. Cell *83*, 793-802.

Grell, M., Wajant, H., Zimmermann, G., and Scheurich, P. (1998). The type 1 receptor (CD120a) is the high-affinity receptor for soluble tumor necrosis factor. Proc Natl Acad Sci U S A *95*, 570-575.

Han, J., and Zuniga-Pflucker, J.C. (2021). A 2020 View of Thymus Stromal Cells in T Cell Development. J Immunol *206*, 249-256.

1221 Hao, Q.L., Zhu, J., Price, M.A., Payne, K.J., Barsky, L.W., and Crooks, G.M. (2001).
1222 Identification of a novel, human multilymphoid progenitor in cord blood. Blood *97*, 3683-3690.
1223
1224 Hao, Y., Hao, S., Andersen-Nissen, E., Mauck, W.M., 3rd, Zheng, S., Butler, A., Lee, M.J.,
1225 Wilk, A.J., Darby, C., Zager, M.*, et al.* (2021). Integrated analysis of multimodal single-cell
1226 data. Cell *184*, 3573-3587 e3529.
1227
1228 Heinz, S., Benner, C., Spann, N., Bertolino, E., Lin, Y.C., Laslo, P., Cheng, J.X., Murre, C.,
1229 Singh, H., and Glass, C.K. (2010). Simple combinations of lineage-determining transcription
1230 factors prime cis-regulatory elements required for macrophage and B cell identities. Mol Cell
1231 *38*, 576-589.
1232
1233 Hoebeke, I., De Smedt, M., Stolz, F., Pike-Overzet, K., Staal, F.J., Plum, J., and Leclercq, G.
1234 (2007). T-, B- and NK-lymphoid, but not myeloid cells arise from human CD34(+)CD38(-
1235)CD7(+) common lymphoid progenitors expressing lymphoid-specific genes. Leukemia *21*,
1236 311-319.
1237
1238 Hozumi, K., Mailhos, C., Negishi, N., Hirano, K., Yahata, T., Ando, K., Zuklys, S., Hollander,
1239 G.A., Shima, D.T., and Habu, S. (2008). Delta-like 4 is indispensable in thymic environment
1240 specific for T cell development. J Exp Med *205*, 2507-2513.
1241
1242 Hu, Y., and Smyth, G.K. (2009). ELDA: extreme limiting dilution analysis for comparing
1243 depleted and enriched populations in stem cell and other assays. J Immunol Methods *347*, 70-
1244 78.

Itoh, K., Tezuka, H., Sakoda, H., Konno, M., Nagata, K., Uchiyama, T., Uchino, H., and Mori, K.J. (1989). Reproducible establishment of hemopoietic supportive stromal cell lines from murine bone marrow. Exp Hematol *17*, 145-153.

Jaleco, A.C., Neves, H., Hooijberg, E., Gameiro, P., Clode, N., Haury, M., Henrique, D., and Parreira, L. (2001). Differential effects of Notch ligands Delta-1 and Jagged-1 in human lymphoid differentiation. J Exp Med *194*, 991-1002.

Kirkling, M.E., Cytlak, U., Lau, C.M., Lewis, K.L., Resteu, A., Khodadadi-Jamayran, A., Siebel, C.W., Salmon, H., Merad, M., Tsirigos, A.*, et al.* (2018). Notch Signaling Facilitates In Vitro Generation of Cross-Presenting Classical Dendritic Cells. Cell Rep *23*, 3658-3672 e3656.

Koch, U., Fiorini, E., Benedito, R., Besseyrias, V., Schuster-Gossler, K., Pierres, M., Manley, N.R., Duarte, A., Macdonald, H.R., and Radtke, F. (2008). Delta-like 4 is the essential, nonredundant ligand for Notch1 during thymic T cell lineage commitment. J Exp Med *205*, 2515-2523.

Kriegler, M., Perez, C., DeFay, K., Albert, I., and Lu, S.D. (1988). A novel form of TNF/cachectin is a cell surface cytotoxic transmembrane protein: ramifications for the complex physiology of TNF. Cell *53*, 45-53.

Langmead, B., and Salzberg, S.L. (2012). Fast gapped-read alignment with Bowtie 2. Nat Methods *9*, 357-359.

Langmead, B., Wilks, C., Antonescu, V., and Charles, R. (2019). Scaling read aligners to hundreds of threads on general-purpose processors. Bioinformatics *35*, 421-432.

Lavaert, M., Liang, K.L., Vandamme, N., Park, J.E., Roels, J., Kowalczyk, M.S., Li, B., Ashenberg, O., Tabaka, M., Dionne, D.*, et al.* (2020). Integrated scRNA-Seq Identifies Human Postnatal Thymus Seeding Progenitors and Regulatory Dynamics of Differentiating Immature Thymocytes. Immunity *52*, 1088-1104 e1086.

Lawrence, M., Huber, W., Pages, H., Aboyoun, P., Carlson, M., Gentleman, R., Morgan, M.T., and Carey, V.J. (2013). Software for computing and annotating genomic ranges. PLoS Comput Biol *9*, e1003118.

Le, J., Park, J.E., Ha, V.L., Luong, A., Branciamore, S., Rodin, A.S., Gogoshin, G., Li, F., Loh, Y.E., Camacho, V.*, et al.* (2020). Single-Cell RNA-Seq Mapping of Human Thymopoiesis Reveals Lineage Specification Trajectories and a Commitment Spectrum in T Cell Development. Immunity *52*, 1105-1118 e1109.

Lee, J., Zhou, Y.J., Ma, W., Zhang, W., Aljoufi, A., Luh, T., Lucero, K., Liang, D., Thomsen, M., Bhagat, G.*, et al.* (2017). Lineage specification of human dendritic cells is marked by IRF8 expression in hematopoietic stem cells and multipotent progenitors. Nat Immunol *18*, 877-888.

Lehmann, J.S., Zhao, A., Sun, B., Jiang, W., and Ji, S. (2017). Multiplex Cytokine Profiling of Stimulated Mouse Splenocytes Using a Cytometric Bead-based Immunoassay Platform. J Vis Exp.

1293 Li, B., and Dewey, C.N. (2011). RSEM: accurate transcript quantification from RNA-Seq data
1294 with or without a reference genome. BMC Bioinformatics *12*, 323.
1295
1296 Love, M.I., Huber, W., and Anders, S. (2014). Moderated estimation of fold change and
1297 dispersion for RNA-seq data with DESeq2. Genome Biol *15*, 550.
1298
1299 Luche, H., Ardouin, L., Teo, P., See, P., Henri, S., Merad, M., Ginhoux, F., and Malissen, B.
1300 (2011). The earliest intrathymic precursors of CD8alpha(+) thymic dendritic cells correspond
1301 to myeloid-type double-negative 1c cells. Eur J Immunol *41*, 2165-2175.
1302
1303 Mace, E.M., Bigley, V., Gunesch, J.T., Chinn, I.K., Angelo, L.S., Care, M.A., Maisuria, S.,
1304 Keller, M.D., Togi, S., Watkin, L.B.*, et al.* (2017). Biallelic mutations in IRF8 impair human
1305 NK cell maturation and function. J Clin Invest *127*, 306-320.
1306
1307 Maney, N.J., Reynolds, G., Krippner-Heidenreich, A., and Hilkens, C.M.U. (2014). Dendritic
1308 cell maturation and survival are differentially regulated by TNFR1 and TNFR2. J Immunol *193*,
1309 4914-4923.
1310
1311 Marquez, C., Trigueros, C., Fernandez, E., and Toribio, M.L. (1995). The development of T
1312 and non-T cell lineages from CD34+ human thymic precursors can be traced by the differential
1313 expression of CD44. J Exp Med *181*, 475-483.
1314
1315 Martin-Gayo, E., Gonzalez-Garcia, S., Garcia-Leon, M.J., Murcia-Ceballos, A., Alcain, J.,
1316 Garcia-Peydro, M., Allende, L., de Andres, B., Gaspar, M.L., and Toribio, M.L. (2017).

Spatially restricted JAG1-Notch signaling in human thymus provides suitable DC developmental niches. J Exp Med *214*, 3361-3379.

Martin-Gayo, E., Sierra-Filardi, E., Corbi, A.L., and Toribio, M.L. (2010). Plasmacytoid dendritic cells resident in human thymus drive natural Treg cell development. Blood *115*, 5366-5375.

Martin, M. (2011). Cutadapt removes adapter sequences from high-throughput sequencing reads. 2011 *17*, 3.

McCarthy, D.J., Campbell, K.R., Lun, A.T., and Wills, Q.F. (2017). Scater: pre-processing, quality control, normalization and visualization of single-cell RNA-seq data in R. Bioinformatics *33*, 1179-1186.

Mclnnes, L., Healy, J., and Melville, J. (2018). UMAP: Uniform Manifold Approximation and Projection for Dimension Reduction. arXiv.

Moirangthem, R.D., Ma, K., Lizot, S., Cordesse, A., Olivre, J., de Chappedelaine, C., Joshi, A., Cieslak, A., Tchen, J., Cagnard, N.*, et al.* (2021). A DL-4- and TNFalpha-based culture system to generate high numbers of nonmodified or genetically modified immunotherapeutic human T-lymphoid progenitors. Cell Mol Immunol.

Montel-Hagen, A., Seet, C.S., Li, S., Chick, B., Zhu, Y., Chang, P., Tsai, S., Sun, V., Lopez, S., Chen, H.C.*, et al.* (2019). Organoid-Induced Differentiation of Conventional T Cells from Human Pluripotent Stem Cells. Cell Stem Cell *24*, 376-389 e378.

1342 Moore, A.J., Sarmiento, J., Mohtashami, M., Braunstein, M., Zuniga-Pflucker, J.C., and
1343 Anderson, M.K. (2012). Transcriptional priming of intrathymic precursors for dendritic cell
1344 development. Development *139*, 373-384.
1345
1346 Nunez, S., Moore, C., Gao, B., Rogers, K., Hidalgo, Y., Del Nido, P.J., Restaino, S., Naka, Y.,
1347 Bhagat, G., Madsen, J.C.*, et al.* (2016). The human thymus perivascular space is a functional
1348 niche for viral-specific plasma cells. Sci Immunol *1*.
1349
1350 Offner, F., Kerre, T., De Smedt, M., and Plum, J. (1999). Bone marrow CD34 cells generate
1351 fewer T cells in vitro with increasing age and following chemotherapy. Br J Haematol *104*, 801-
1352 808.
1353
1354 Palucka, A.K., Blanck, J.P., Bennett, L., Pascual, V., and Banchereau, J. (2005). Cross-
1355 regulation of TNF and IFN-alpha in autoimmune diseases. Proc Natl Acad Sci U S A *102*, 3372-
1356 3377.
1357
1358 Park, J.E., Botting, R.A., Dominguez Conde, C., Popescu, D.M., Lavaert, M., Kunz, D.J., Goh,
1359 I., Stephenson, E., Ragazzini, R., Tuck, E.*, et al.* (2020). A cell atlas of human thymic
1360 development defines T cell repertoire formation. Science *367*.
1361
1362 Parry, S.L., Sebbag, M., Feldmann, M., and Brennan, F.M. (1997). Contact with T cells
1363 modulates monocyte IL-10 production: role of T cell membrane TNF-alpha. J Immunol *158*,
1364 3673-3681.
1365

Patel, E., Wang, B., Lien, L., Wang, Y., Yang, L.J., Moreb, J.S., and Chang, L.J. (2009). Diverse T-cell differentiation potentials of human fetal thymus, fetal liver, cord blood and adult bone marrow CD34 cells on lentiviral Delta-like-1-modified mouse stromal cells. Immunology *128*, e497-505.

Porritt, H.E., Rumfelt, L.L., Tabrizifard, S., Schmitt, T.M., Zuniga-Pflucker, J.C., and Petrie, H.T. (2004). Heterogeneity among DN1 prothymocytes reveals multiple progenitors with different capacities to generate T cell and non-T cell lineages. Immunity *20*, 735-745.

Robinson, M.D., McCarthy, D.J., and Smyth, G.K. (2010). edgeR: a Bioconductor package for differential expression analysis of digital gene expression data. Bioinformatics *26*, 139-140.

Roels, J., Kuchmiy, A., De Decker, M., Strubbe, S., Lavaert, M., Liang, K.L., Leclercq, G., Vandekerckhove, B., Van Nieuwerburgh, F., Van Vlierberghe, P.*, et al.* (2020). Distinct and temporary-restricted epigenetic mechanisms regulate human alphabeta and gammadelta T cell development. Nat Immunol *21*, 1280-1292.

Rothenberg, E.V. (2021). Single-cell insights into the hematopoietic generation of T-lymphocyte precursors in mouse and human. Exp Hematol *95*, 1-12.

Schmitt, T.M., and Zuniga-Pflucker, J.C. (2002). Induction of T cell development from hematopoietic progenitor cells by delta-like-1 in vitro. Immunity *17*, 749-756.

1389 Seet, C.S., He, C., Bethune, M.T., Li, S., Chick, B., Gschweng, E.H., Zhu, Y., Kim, K., Kohn,
1390 D.B., Baltimore, D., *et al.* (2017). Generation of mature T cells from human hematopoietic stem
1391 and progenitor cells in artificial thymic organoids. Nat Methods *14*, 521-530.
1392
1393 Senyuk, V., Patel, P., Mahmud, N., and Rondelli, D. (2018). Blockade of TNFalpha to Improve
1394 Human CD34+ Cell Repopulating Activity in Allogeneic Stem Cell Transplantation. Front
1395 Immunol *9*, 3186.
1396
1397 Shyamsunder, P., Shanmugasundaram, M., Mayakonda, A., Dakle, P., Teoh, W.W., Han, L.,
1398 Kanojia, D., Lim, M.C., Fullwood, M., An, O., *et al.* (2019). Identification of a novel enhancer
1399 of CEBPE essential for granulocytic differentiation. Blood *133*, 2507-2517.
1400
1401 Silva, A., Yunes, J.A., Cardoso, B.A., Martins, L.R., Jotta, P.Y., Abecasis, M., Nowill, A.E.,
1402 Leslie, N.R., Cardoso, A.A., and Barata, J.T. (2008). PTEN posttranslational inactivation and
1403 hyperactivation of the PI3K/Akt pathway sustain primary T cell leukemia viability. J Clin Invest
1404 *118*, 3762-3774.
1405
1406 Smits, K., De Smedt, M., Naessens, E., De Smet, G., Stove, V., Taghon, T., Plum, J., and
1407 Verhasselt, B. (2007). Tumor necrosis factor promotes T-cell at the expense of B-cell lymphoid
1408 development from cultured human CD34+ cord blood cells. Exp Hematol *35*, 1272-1278.
1409
1410 Sontag, S., Forster, M., Qin, J., Wanek, P., Mitzka, S., Schuler, H.M., Koschmieder, S., Rose-
1411 John, S., Sere, K., and Zenke, M. (2017). Modelling IRF8 Deficient Human Hematopoiesis and
1412 Dendritic Cell Development with Engineered iPS Cells. Stem Cells *35*, 898-908.

1413 Swat, W., Montgrain, V., Doggett, T.A., Douangpanya, J., Puri, K., Vermi, W., and Diacovo,
1414 T.G. (2006). Essential role of PI3Kdelta and PI3Kgamma in thymocyte survival. Blood *107*,
1415 2415-2422.
1416
1417 Taghon, T., De Smedt, M., Stolz, F., Cnockaert, M., Plum, J., and Leclercq, G. (2001). Enforced
1418 expression of GATA-3 severely reduces human thymic cellularity. J Immunol *167*, 4468-4475.
1419
1420 Taghon, T., Stolz, F., De Smedt, M., Cnockaert, M., Verhasselt, B., Plum, J., and Leclercq, G.
1421 (2002). HOX-A10 regulates hematopoietic lineage commitment: evidence for a monocyte-
1422 specific transcription factor. Blood *99*, 1197-1204.
1423
1424 Taghon, T., Waegemans, E., and Van de Walle, I. (2012). Notch signaling during human T cell
1425 development. Curr Top Microbiol Immunol *360*, 75-97.
1426
1427 Van de Walle, I., Davids, K., and Taghon, T. (2016a). Characterization and Isolation of Human
1428 T Cell Progenitors. Methods Mol Biol *1323*, 221-237.
1429
1430 Van de Walle, I., De Smet, G., De Smedt, M., Vandekerckhove, B., Leclercq, G., Plum, J., and
1431 Taghon, T. (2009). An early decrease in Notch activation is required for human TCR-alphabeta
1432 lineage differentiation at the expense of TCR-gammadelta T cells. Blood *113*, 2988-2998.
1433
1434 Van de Walle, I., De Smet, G., Gartner, M., De Smedt, M., Waegemans, E., Vandekerckhove,
1435 B., Leclercq, G., Plum, J., Aster, J.C., Bernstein, I.D.*, et al.* (2011). Jagged2 acts as a Delta-like
1436 Notch ligand during early hematopoietic cell fate decisions. Blood *117*, 4449-4459.

1437 Van de Walle, I., Dolens, A.C., Durinck, K., De Mulder, K., Van Loocke, W., Damle, S.,
1438 Waegemans, E., De Medts, J., Velghe, I., De Smedt, M.*, et al.* (2016b). GATA3 induces human
1439 T-cell commitment by restraining Notch activity and repressing NK-cell fate. Nat Commun *7*,
1440 11171.
1441
1442 Watanabe, N., Wang, Y.H., Lee, H.K., Ito, T., Cao, W., and Liu, Y.J. (2005). Hassall's
1443 corpuscles instruct dendritic cells to induce CD4+CD25+ regulatory T cells in human thymus.
1444 Nature *436*, 1181-1185.
1445
1446 Weber, B.N., Chi, A.W., Chavez, A., Yashiro-Ohtani, Y., Yang, Q., Shestova, O., and
1447 Bhandoola, A. (2011). A critical role for TCF-1 in T-lineage specification and differentiation.
1448 Nature *476*, 63-68.
1449
1450 Weekx, S.F., Snoeck, H.W., Offner, F., De Smedt, M., Van Bockstaele, D.R., Nijs, G., Lenjou,
1451 M., Moulijn, A., Rodrigus, I., Berneman, Z.N.*, et al.* (2000). Generation of T cells from adult
1452 human hematopoietic stem cells and progenitors in a fetal thymic organ culture system:
1453 stimulation by tumor necrosis factor-alpha. Blood *95*, 2806-2812.
1454
1455 Xu, H., Zhu, J., Smith, S., Foldi, J., Zhao, B., Chung, A.Y., Outtz, H., Kitajewski, J., Shi, C.,
1456 Weber, S.*, et al.* (2012). Notch-RBP-J signaling regulates the transcription factor IRF8 to
1457 promote inflammatory macrophage polarization. Nat Immunol *13*, 642-650.
1458
1459 Xue, L., Chiang, L., Kang, C., and Winoto, A. (2008). The role of the PI3K-AKT kinase
1460 pathway in T-cell development beyond the beta checkpoint. Eur J Immunol *38*, 3200-3207.

Yui, M.A., Feng, N., and Rothenberg, E.V. (2010). Fine-scale staging of T cell lineage commitment in adult mouse thymus. J Immunol *185*, 284-293.

Zeng, Y., Liu, C., Gong, Y., Bai, Z., Hou, S., He, J., Bian, Z., Li, Z., Ni, Y., Yan, J.*, et al.* (2019). Single-Cell RNA Sequencing Resolves Spatiotemporal Development of Pre-thymic Lymphoid Progenitors and Thymus Organogenesis in Human Embryos. Immunity *51*, 930-948 e936.

Zhou, W., Yui, M.A., Williams, B.A., Yun, J., Wold, B.J., Cai, L., and Rothenberg, E.V. (2019). Single-Cell Analysis Reveals Regulatory Gene Expression Dynamics Leading to Lineage Commitment in Early T Cell Development. Cell Syst *9*, 321-337 e329.

Zielske, S.P., and Braun, S.E. (2004). Cytokines: value-added products in hematopoietic stem cell gene therapy. Mol Ther *10*, 211-219.

Figure 1

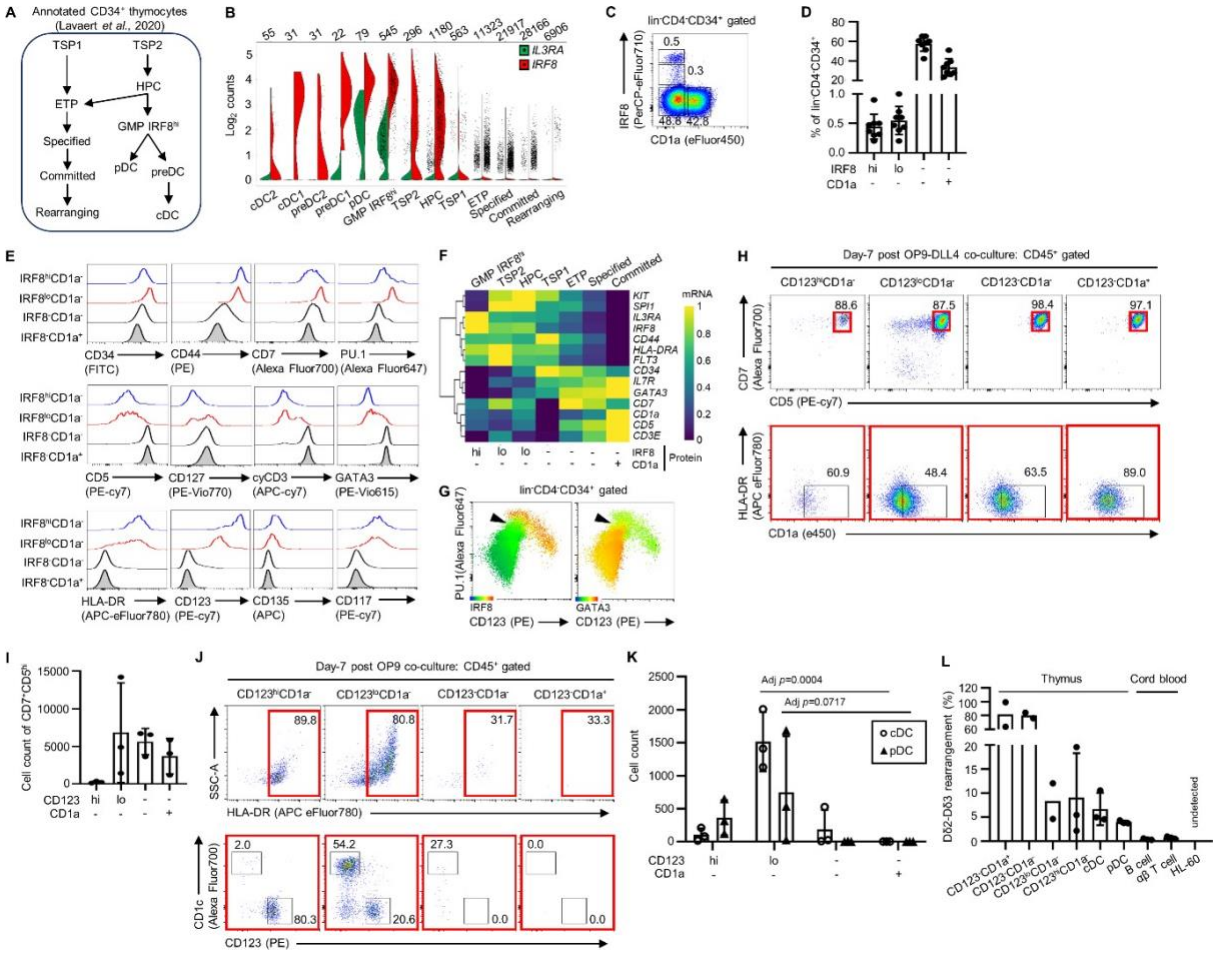
A
Annotated CD34+ thymocytes
(Lavaert et al., 2020)
TSP1
TSP2
HPC
ETP
GMP IRF8lo
Specified
pDC
preDC
Committed
Rearranging
cDC
B
Log2 counts
IL3RA
IRF8
cDC2
cDC1
preDC2
preDC1
pDC
GMP IRF8lo
TSP2
HPC
TSP1
ETP
Specified
Committed
Rearranging
C
lin-CD4-CD34+ gated
IRF8 (PerCP-eFluor710)
CD1a (eFluor450)
D
% of lin-CD4-CD34+
E
CD34 (FITC)
CD44 (PE)
CD7 (Alexa Fluor700)
PU.1 (Alexa Fluor647)
CD5 (PE-cy7)
CD127 (PE-Vio770)
cyCD3 (APC-cy7)
GATA3 (PE-Vio615)
HLA-DR (APC-eFluor780)
CD123 (PE-cy7)
CD135 (APC)
CD117 (PE-cy7)
F
mRNA
KIT
SPI1
IL3RA
IRF8
CD44
HLA-DRA
FLT3
CD34
IL7R
GATA3
CD7
CD1a
CD5
CD3E
Protein
G
lin-CD4-CD34+ gated
PU.1 (Alexa Fluor647)
CD123 (PE)
GATA3
H
Day-7 post OP9-DLL4 co-culture: CD45+ gated
CD7 (Alexa Fluor700)
CD5 (PE-cy7)
HLA-DR (APC-eFluor780)
CD1a (e450)
I
Cell count of CD7-CD5lo
J
Day-7 post OP9 co-culture: CD45+ gated
SSC-A
HLA-DR (APC eFluor780)
CD1c (Alexa Fluor700)
CD123 (PE)
K
Cell count
Adj p=0.0004
Adj p=0.0717
cDC
pDC
L
Thymus
Cord blood
DJ-DJ rearrangement (%)
undetected

1479 **Figure 2**

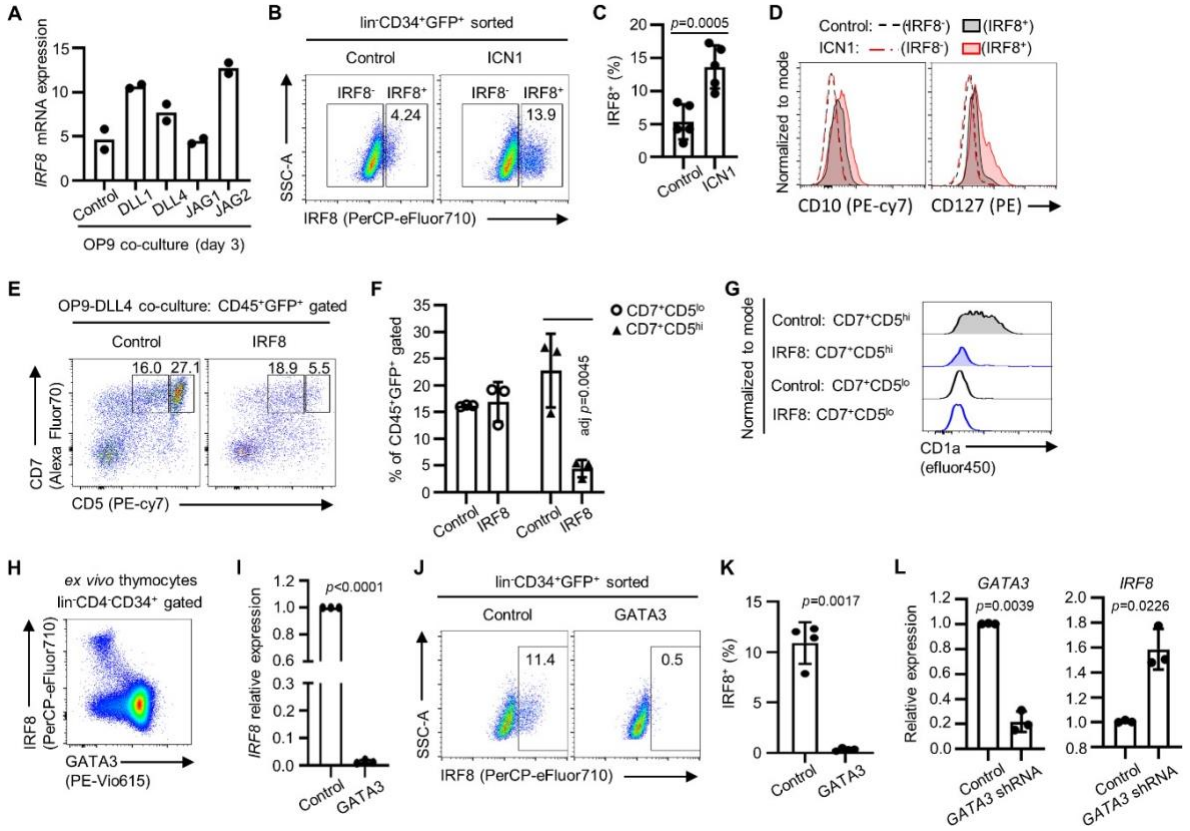

1480

1481

Figure 3

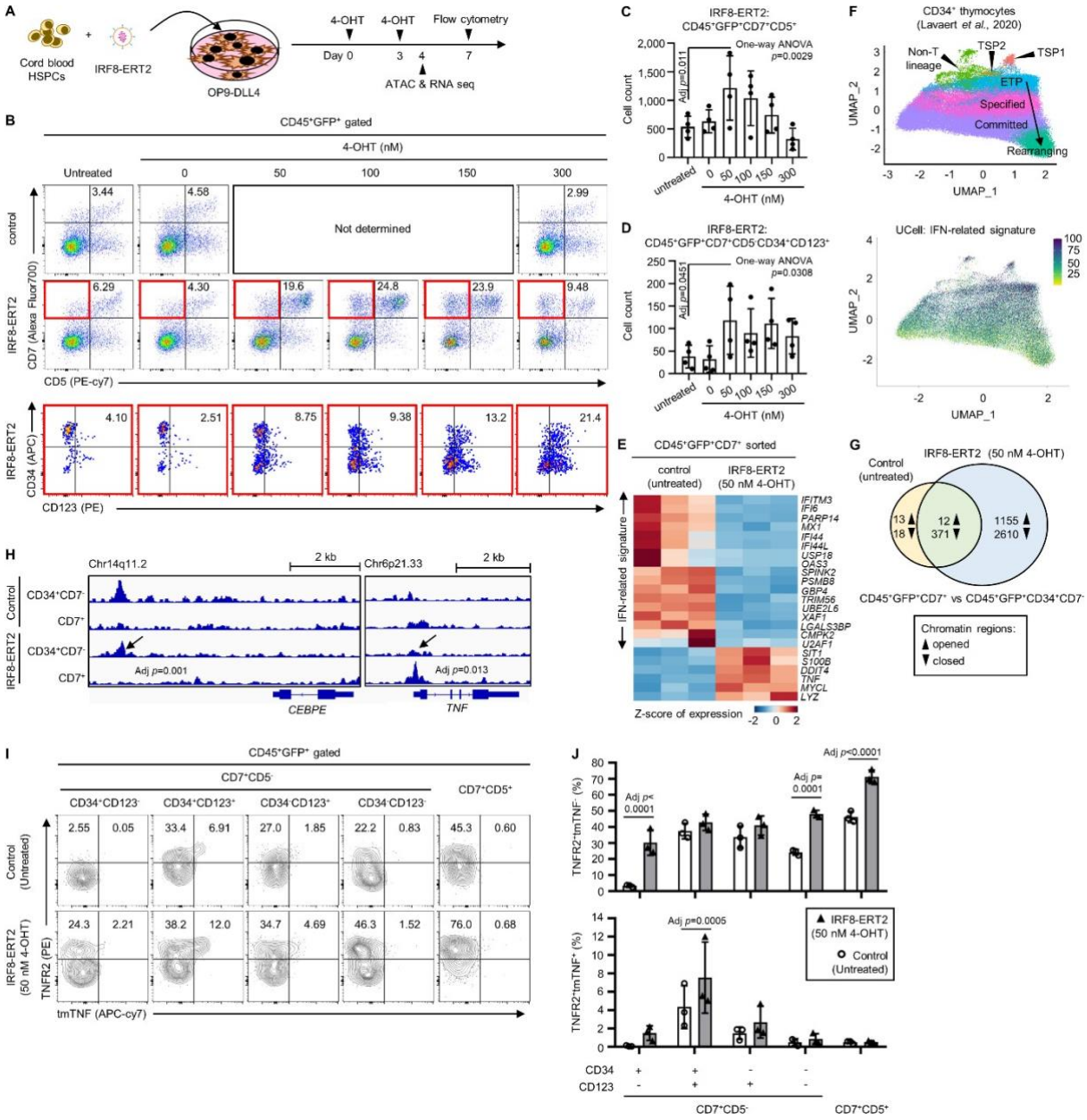
A
Cord blood HSPCs
IRF8-ERT2
OP9-DLL4
4-OHT
4-OHT
Flow cytometry
Day 0
3
4
7
ATAC & RNA seq
B
CD45+GFP+ gated
4-OHT (nM)
Untreated
0
50
100
150
300
control
IRF8-ERT2
CD7 (Alexa Fluor700)
CD5 (PE-cy7)
Not determined
3.44
4.58
2.99
6.29
4.30
19.6
24.8
23.9
9.48
IRF8-ERT2
CD34 (APC)
CD123 (PE)
4.10
2.51
8.75
9.38
13.2
21.4
C
IRF8-ERT2:
CD45+GFP+CD7+CD5+
One-way ANOVA
p=0.0029
Adj p=0.011
Cell count
4-OHT (nM)
D
IRF8-ERT2:
CD45+GFP+CD7+CD5-CD34+CD123+
One-way ANOVA
p=0.0308
Adj p=0.0451
Cell count
4-OHT (nM)
E
CD45+GFP+CD7+ sorted
control (untreated)
IRF8-ERT2 (50 nM 4-OHT)
IFN-related signature
IFITM3
IFI6
PARP14
MX1
IFI44
IFI44L
USP18
OAS3
SPINK2
PSMB8
GBP4
TRIM56
UBE2L6
XAF1
LGALS3BP
CMPK2
U2AF1
SIT1
S100B
DDIT4
TNF
MYCL
LYZ
Z-score of expression
F
CD34+ thymocytes
(Lavaert et al., 2020)
Non-T lineage
TSP2
TSP1
ETP
Specified
Committed
Rearranging
UMAP_2
UMAP_1
UCell: IFN-related signature
G
IRF8-ERT2 (50 nM 4-OHT)
Control (untreated)
13
18
12
371
1155
2610
CD45+GFP+CD7+ vs CD45+GFP+CD34+CD7-
Chromatin regions:
opened
closed
H
Chr14q11.2
2 kb
Chr6p21.33
2 kb
Control
IRF8-ERT2
CD34+CD7-
CD7+
Adj p=0.001
Adj p=0.013
CEBPE
TNF
I
CD45+GFP+ gated
CD7+CD5-
CD7+CD5+
CD34+CD123-
CD34+CD123+
CD34-CD123+
CD34-CD123-
Control (Untreated)
IRF8-ERT2 (50 nM 4-OHT)
TNFR2 (PE)
tmTNF (APC-cy7)
2.55
0.05
33.4
6.91
27.0
1.85
22.2
0.83
45.3
0.60
24.3
2.21
38.2
12.0
34.7
4.69
46.3
1.52
76.0
0.68
J
TNFR2+tmTNF+ (%)
Adj p< 0.0001
Adj p= 0.0001
Adj p<0.0001
Adj p=0.0005
IRF8-ERT2 (50 nM 4-OHT)
Control (Untreated)
CD34
CD123
CD7+CD5-
CD7+CD5+

Figure 4

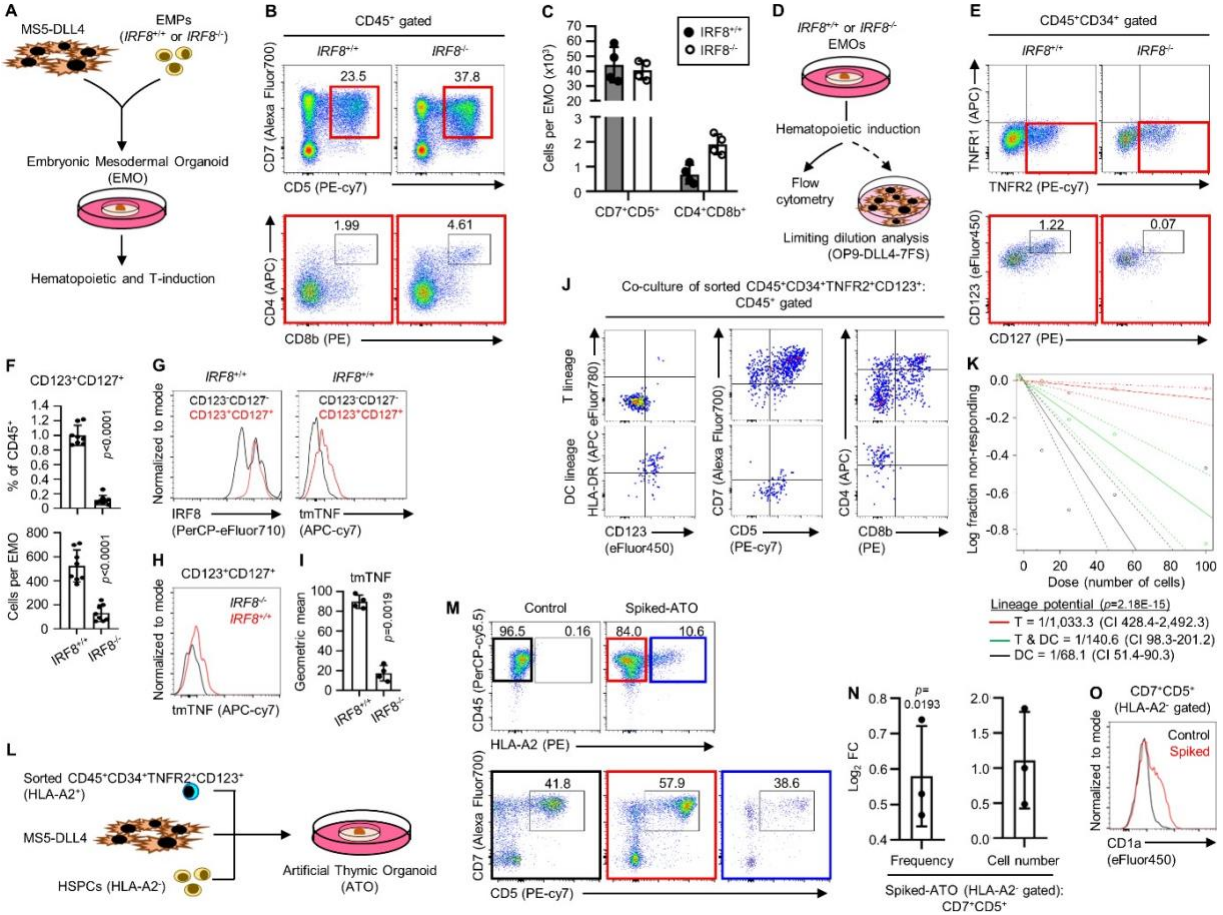
A
MS5-DLL4
EMPs
(IRF8+/+ or IRF8-/-)
Embryonic Mesodermal Organoid
(EMO)
Hematopoietic and T-induction
B
CD45+ gated
IRF8+/+
IRF8-/-
23.5
37.8
CD7 (Alexa Fluor700)
CD5 (PE-cy7)
1.99
4.61
CD4 (APC)
CD8b (PE)
C
Cells per EMO (x10³)
IRF8+/+
IRF8-/-
CD7+CD5+
CD4+CD8b+
D
IRF8+/+ or IRF8-/-
EMOs
Hematopoietic induction
Flow cytometry
Limiting dilution analysis
(OP9-DLL4-7FS)
E
CD45+CD34+ gated
IRF8+/+
IRF8-/-
TNFR1 (APC)
TNFR2 (PE-cy7)
1.22
0.07
CD123 (eFluor450)
CD127 (PE)
F
CD123+CD127+
% of CD45+
p<0.0001
Cells per EMO
p<0.0001
IRF8+/+
IRF8-/-
G
IRF8+/+
IRF8+/+
CD123-CD127-
CD123+CD127+
Normalized to mode
IRF8
(PerCP-eFluor710)
tmTNF
(APC-cy7)
H
CD123+CD127+
IRF8-/-
IRF8+/+
Normalized to mode
tmTNF (APC-cy7)
I
tmTNF
Geometric mean
p=0.0019
IRF8+/+
IRF8-/-
J
Co-culture of sorted CD45+CD34+TNFR2+CD123+:
CD45+ gated
T lineage
DC lineage
HLA-DR (APC-eFluor780)
CD123
(eFluor450)
CD7 (Alexa Fluor700)
CD5
(PE-cy7)
CD4 (APC)
CD8b
(PE)
K
Log fraction non-responding
Dose (number of cells)
Lineage potential (p=2.18E-15)
T = 1/1,033.3 (CI 428.4-2,492.3)
T & DC = 1/140.6 (CI 98.3-201.2)
DC = 1/68.1 (CI 51.4-90.3)
L
Sorted CD45+CD34+TNFR2+CD123+
(HLA-A2+)
MS5-DLL4
HSPCs (HLA-A2-)
Artificial Thymic Organoid
(ATO)
M
Control
Spiked-ATO
96.5
0.16
84.0
10.6
CD45 (PerCP-cy5.5)
HLA-A2 (PE)
41.8
57.9
38.6
CD7 (Alexa Fluor700)
CD5 (PE-cy7)
N
p=
0.0193
Log2 FC
Frequency
Cell number
Spiked-ATO (HLA-A2- gated):
CD7+CD5+
O
CD7+CD5+
(HLA-A2- gated)
Control
Spiked
Normalized to mode
CD1a
(eFluor450)

Figure 5

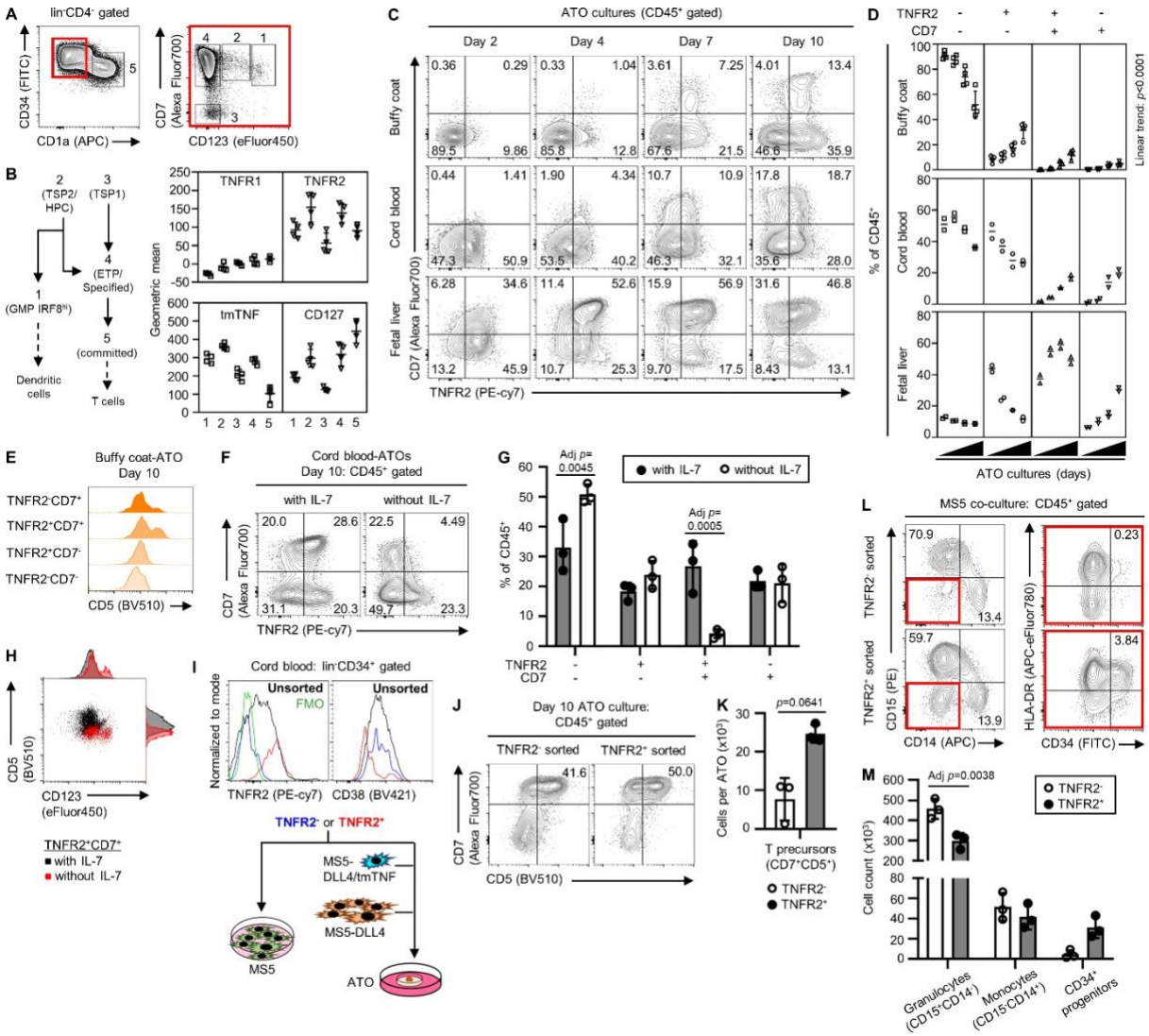
A
lin-CD4- gated
CD34 (FITC)
CD1a (APC)
CD7 (Alexa Fluor700)
CD123 (eFluor450)
B
2 (TSP2/ HPC)
3 (TSP1)
1 (GMP IRF8hi)
4 (ETP/ Specified)
5 (committed)
Dendritic cells
T cells
Geometric mean
TNFR1
TNFR2
tmTNF
CD127
C
ATO cultures (CD45+ gated)
Day 2
Day 4
Day 7
Day 10
Buffy coat
Cord blood
Fetal liver
CD7 (Alexa Fluor700)
TNFR2 (PE-cy7)
D
TNFR2
CD7
% of CD45-
Buffy coat
Cord blood
Fetal liver
Linear trend: p<0.0001
ATO cultures (days)
E
Buffy coat-ATO Day 10
TNFR2-CD7+
TNFR2+CD7+
TNFR2+CD7-
TNFR2-CD7-
CD5 (BV510)
F
Cord blood-ATOs Day 10: CD45+ gated
with IL-7
without IL-7
CD7 (Alexa Fluor700)
TNFR2 (PE-cy7)
G
Adj p= 0.0045
Adj p= 0.0005
with IL-7
without IL-7
% of CD45+
TNFR2
CD7
H
CD5 (BV510)
CD123 (eFluor450)
TNFR2+CD7+
with IL-7
without IL-7
I
Cord blood: lin-CD34+ gated
Unsorted
FMO
Normalized to mode
TNFR2 (PE-cy7)
CD38 (BV421)
TNFR2- or TNFR2+
MS5-DLL4/tmTNF
MS5-DLL4
MS5
ATO
J
Day 10 ATO culture: CD45+ gated
TNFR2- sorted
TNFR2+ sorted
CD7 (Alexa Fluor700)
CD5 (BV510)
K
p=0.0641
Cells per ATO (x10³)
T precursors (CD7+CD5+)
TNFR2-
TNFR2+
L
MS5 co-culture: CD45+ gated
TNFR2- sorted
TNFR2+ sorted
CD15 (PE)
CD14 (APC)
HLA-DR (APC-eFluor780)
CD34 (FITC)
M
Adj p=0.0038
TNFR2-
TNFR2+
Cell count (x10³)
Granulocytes (CD15+CD14+)
Monocytes (CD15-CD14+)
CD34+ progenitors

1492 **Figure 6**

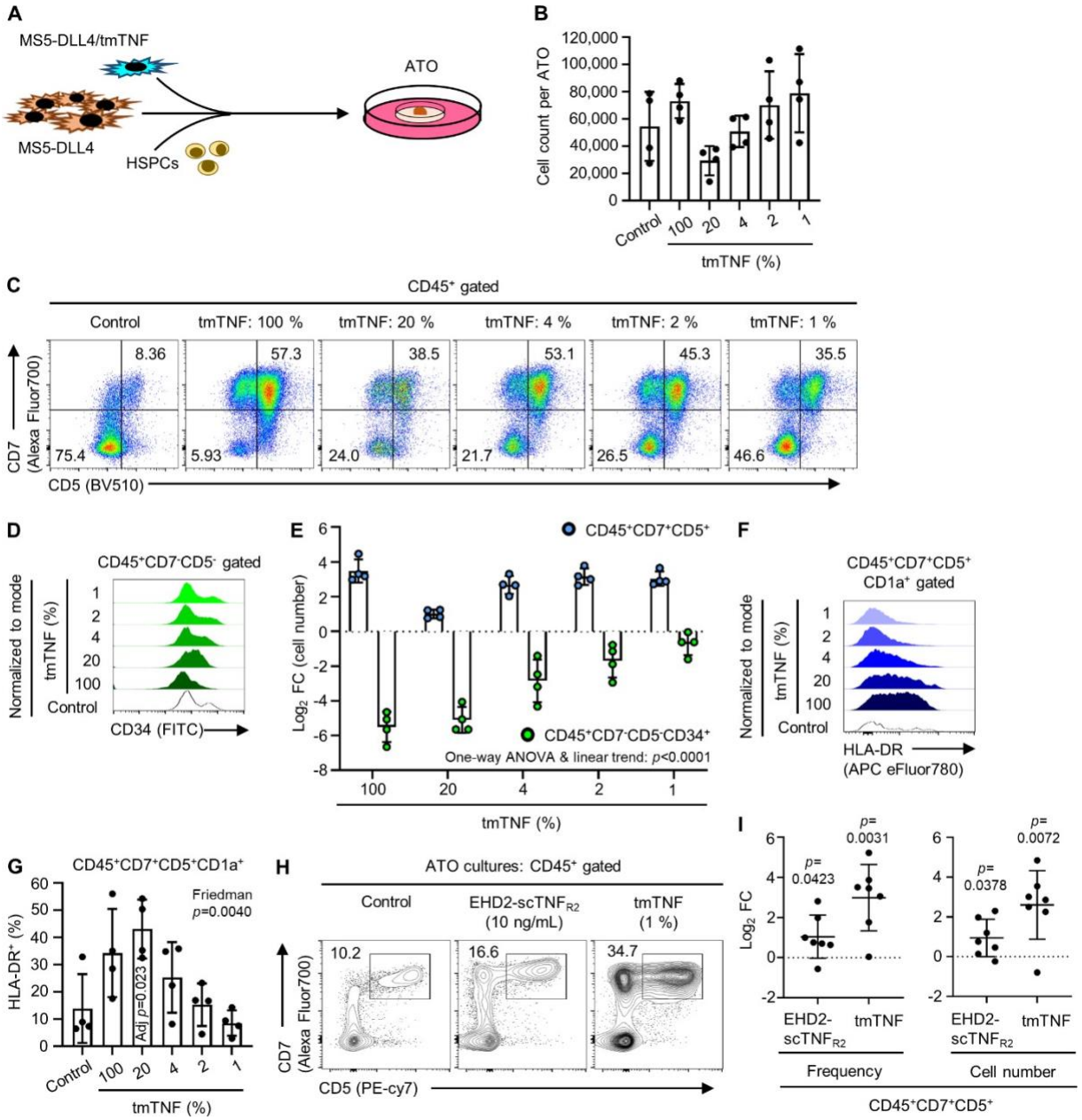

1493

1494

Figure 7

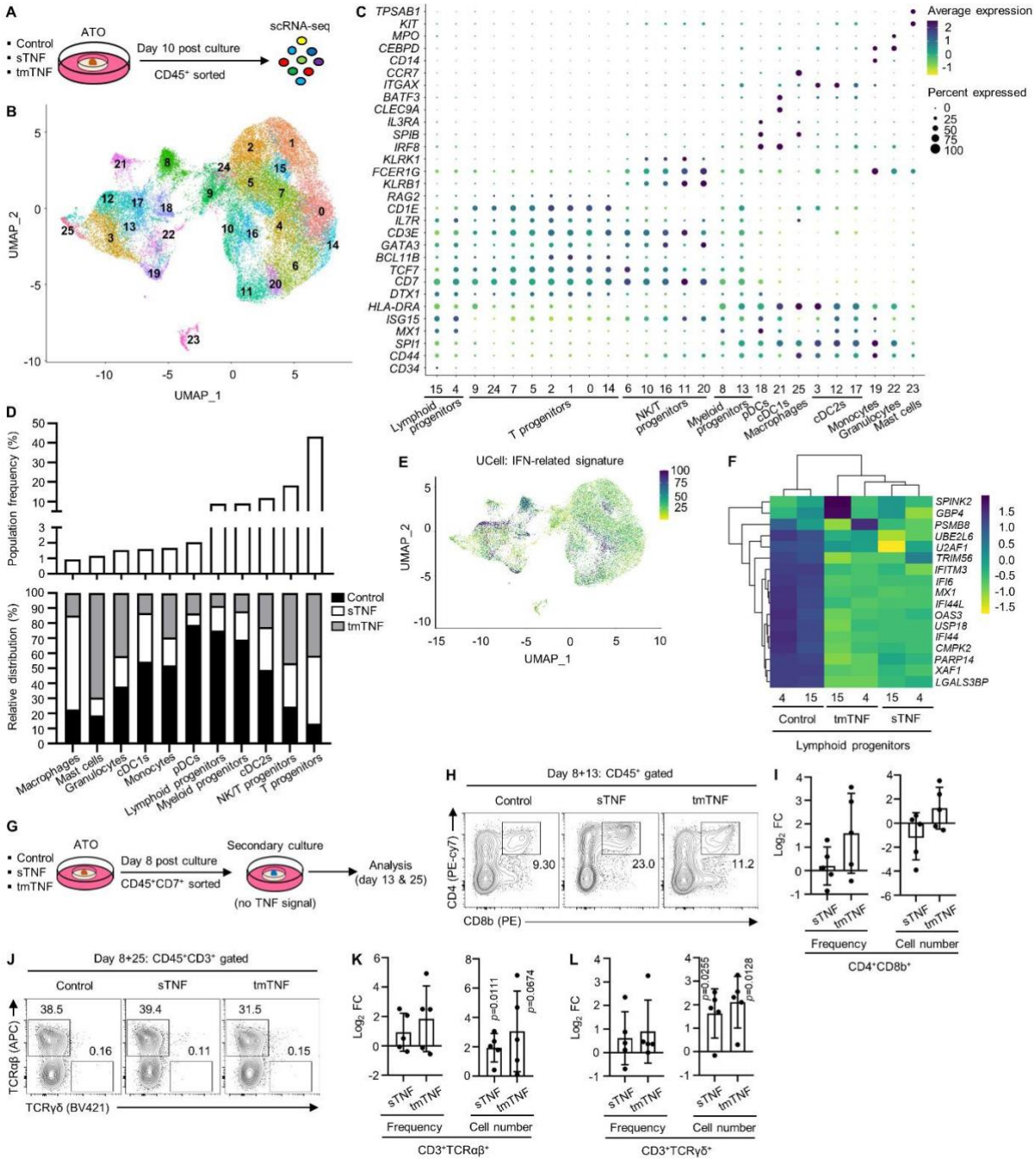
A
Control
sTNF
tmTNF
ATO
Day 10 post culture
CD45+ sorted
scRNA-seq
B
UMAP_1
UMAP_2
C
Average expression
Percent expressed
Lymphoid progenitors
T progenitors
NK/T progenitors
Myeloid progenitors
pDCs
cDC1s
Macrophages
cDC2s
Monocytes
Granulocytes
Mast cells
D
Population frequency (%)
Relative distribution (%)
Control
sTNF
tmTNF
E
UCell: IFN-related signature
F
Control
tmTNF
sTNF
Lymphoid progenitors
G
Day 8 post culture
CD45+CD7+ sorted
Secondary culture
(no TNF signal)
Analysis (day 13 & 25)
H
Day 8+13: CD45+ gated
CD4 (PE-cy7)
CD8b (PE)
9.30
23.0
11.2
I
Log2 FC
Frequency
Cell number
CD4+CD8b+
J
Day 8+25: CD45+CD3+ gated
TCRαβ (APC)
TCRγδ (BV421)
38.5
0.16
39.4
0.11
31.5
0.15
K
p=0.0111
p=0.0674
CD3+TCRαβ+
L
p=0.0255
p=0.0128
CD3+TCRγδ+